Magmatic Cu-Ni-PGE-Au sulfide mineralisation in alkaline igneous systems: An example from the Sron Garbh intrusion, Tyndrum, Scotland

S.D. Graham [a,b], D.A. Holwell [a,*], I. McDonald [c], G.R.T. Jenkin [a], N.J. Hill [a,d], A.J. Boyce [e], J. Smith [d], C. Sangster [d]

[a] Department of Geology, University of Leicester, University Road, Leicester LE1 7RH, UK
[b] Carl Zeiss Microscopy Ltd, 509 Coldhams Lane, Cambridge CB1 3JS, UK
[c] School of Earth & Ocean Sciences, Cardiff University, Cardiff CF10 3AT, UK
[d] Scotgold Resources Limited, Upper Station, Tyndrum, Stirlingshire FK20 8RY, UK
[e] Scottish Universities Environmental Research Centre, Rankine Avenue, Scottish Enterprise Technology Park, East Kilbride G75 0QF, UK

ARTICLE INFO

ABSTRACT

Magmatic sulfide deposits typically occur in ultramafic-mafic systems, however, mineralisation can occur in more intermediate and alkaline magmas. Sron Garbh is an appinite-diorite intrusion emplaced into Dalradian metasediments in the Tyndrum area of Scotland that hosts magmatic Cu-Ni-PGE-Au sulfide mineralisation in the appinitic portion. It is thus an example of magmatic sulfide mineralisation hosted by alkaline rocks, and is the most significantly mineralised appinitic intrusion known in the British Isles. The intrusion is irregularly shaped, with an appinite rim, comprising amphibole cumulates classed as vogesites. The central portion of the intrusion is comprised of unmineralised, but pyrite-bearing, diorites. Both appinites and diorites have similar trace element geochemistry that suggests the diorite is a more fractionated differentiate of the appinite from a common source that can be classed with the high Ba-Sr intrusions of the Scottish Caledonides. Mineralisation is present as a disseminated, primary chalcopyrite-pyrite-PGM assemblage and a blebby, pyrite-chalcopyrite assemblage with significant Co-As-rich pyrite. Both assemblages contain minor millerite and Ni-Co-As-sulfides. The mineralisation is Cu-, PPGE-, and Au-rich and IPGE-poor and the platinum group mineral assemblage is overwhelmingly dominated by Pd minerals; however, the bulk rock Pt/Pd ratio is around 0.8. Laser ablation analysis of the sulfides reveals that pyrite and the Ni-Co-sulfides are the primary host for Pt, which is present in solid solution in concentrations of up to 22 ppm in pyrite. Good correlations between all base and precious metals indicate very little hydrothermal remobilisation of metals despite some evidence of secondary pyrite and PGM. Sulfur isotope data indicate some crustal S in the magmatic sulfide assemblages. The source of this is unlikely to have been the local quartzites, but S-rich Dalradian sediments present at depth. The generation of magmatic Cu-Ni-PGE-Au mineralisation at Sron Garbh can be attributed to post-collisional slab drop off that allowed hydrous, low-degree partial melting to take place that produced a Cu-PPGE-Au-enriched melt, which ascended through the crust, assimilating crustal S from the Dalradian sediments. The presence of a number of PGE-enriched sulfide occurrences in appinitic intrusions across the Scottish Caledonides indicates that the region contains certain features that make it more prospective than other alkaline provinces worldwide, which may be linked the post-Caledonian slab drop off event. We propose that the incongruent melting of pre-existing magmatic sulfides or 'refertilised' mantle in low-degree partial melts can produce characteristically fractionated, Cu-PPGE-Au-semi metal bearing, hydrous, alkali melts, which, if they undergo sulfide saturation, have the potential to produce alkaline-hosted magmatic sulfide deposits.

1. Introduction

Typical magmatic Ni-Cu-platinum-group element (PGE) sulfide deposits occur in five major settings in magmatic systems that are almost exclusively ultramafic-mafic in their composition (e.g. Maier, 2005; Naldrett, 2011; Barnes et al., 2016): (1) stratiform reef style deposits mostly in the lower parts of layered intrusions, often linked with magma mixing (e.g. Merensky Reef, Bushveld Complex; J-M Reef, Stillwater Complex; Naldrett, 2011; Naldrett et al., 2011; Campbell et al., 1983); (2) deposits located in the conduits and along the margins of such intrusions, often linked with crustal contamination (e.g. Noril'sk, Voisey's Bay; Naldrett, 2011; Ripley and Li, 2011; Arndt, 2011); (3) sulfide disseminations, commonly PGE-rich, in the marginal facies of large layered intrusions; the Platreef of the Bushveld Complex is the type example (McDonald and Holwell, 2011); (4) accumulations of widely varying proportions of sulfide in komatiite lava flows (e.g., Barnes,

2006; Lesher, 1989; Lesher and Keays, 2002) or associated shallow subvolcanic intrusions; and (5) in the unique impact melt setting of the Sudbury Igneous Complex (e.g. Keays and Lightfoot, 2004). The presence of magmatic Ni-Cu-PGE mineralisation in appinitic/lamprophyric intrusions that are more intermediate and alkaline in their composition represents a poorly documented and highly unusual setting for such deposits; though they have been noted in the Mordor Alkaline Igneous Complex, Australia (Barnes et al., 2008).

Appinite intrusions are located throughout the Scottish and Irish Dalradian belt and are considered a characteristic feature of the post-Caledonian magmatism of the region (e.g. Fowler and Henney, 1996). The ultrabasic-intermediate composition appinites are usually considered to be the plutonic equivalents of hornblende-rich lamprophyres (vogesites and spessartite), are often misclassified as diorites, and are associated with granitic intrusions (Barnes et al., 1986; Power et al., 2004). In Scotland, these appinite-diorite intrusions are part of the Argyll and Northern Highlands intrusive suites, which belong to a high Ba-Sr (HiBaSr) sub-class of igneous rocks (Tarney and Jones, 1994 and references therein). They are interpreted to be related to a post-collisional, regional-scale slab drop-off event commencing at c. 430 Ma (Neilson et al., 2009). Rare examples of the alkaline intrusions of similar age containing magmatic Cu-Ni-PGE mineralisation occur in southern Scotland at Talnotry (Power et al., 2004) and at Loch Ailsh and Loch Borralan in the Moine Thrust belt of northern Scotland (Gunn and Styles, 2002; Fig. 1). In this paper, we describe a previously unidentified Cu-Ni-PGE-Au mineralised appinite-diorite intrusion in the Tyndrum area of Scotland at Sron Garbh.

This study provides the first description and classification of the field relations, petrology, base and precious metal mineralogy and geochemistry of the Sron Garbh appinite intrusion and its Cu-Ni-PGE-Au mineralisation. In combination with an S-isotope study of sulfides in the intrusion and the country rocks, we are able to provide a number

of constraints on a petrogenetic and emplacement model for Sron Garbh. The significance of this occurrence of mineralised appinite is then discussed in terms of the implications for PGE mineralisation in similar systems throughout the Caledonides of the British Isles, and lamprophyric magmas in general. We propose a model for PGE-enrichment in these alkaline systems to be primarily linked to slab drop off and hydrous remelting of mantle wedge material.

2. Regional geological setting

The Sron Garbh intrusion is located in Glen Orchy, in the Scottish Caledonides, and is part of a suite of magmatic intrusions across northern Britain emplaced into the Dalradian Supergroup (Fig. 1) during a regional episode of widespread post-collisional (Tarney and Jones, 1994) magmatism c. 430–408 Ma (Neilson et al., 2009). The Dalradian Supergroup is composed of marine clastic sediments with occasional carbonate and volcanic horizons, and has a depositional history ranging from c. 800 Ma in the Neoproterozoic (Cryogenian) to c. 510 Ma in the mid-Cambrian (Cowie et al., 1972; Tanner and Sutherland, 2007; Stephenson et al., 2013). The Dalradian sequence in the Grampian Terrane (Fig. 1) is composed of: (1) the Grampian Group, comprising psammites and semi-pelites deposited in an extensional basin; (2) the Appin Group: a limestone-pelite-quartzite assemblage from a stable shelf environment (Wright, 1988); (3) the Argyll Group, composed of black slate, graphitic schist, mafic lavas and sills, and coarse turbidite sequences (Anderton, 1985) with some locally developed sedimentary exhalative (SEDEX) mineralisation (Stephenson et al., 2013); and (4) the Southern Highland Group of greywackes with volcaniclastic green beds.

The Dalradian Supergroup underwent polyphase deformation during the earliest phase of the Caledonian Orogeny: the Grampian event (e.g. Soper et al., 1992) in the mid Ordovician. This was responsible for
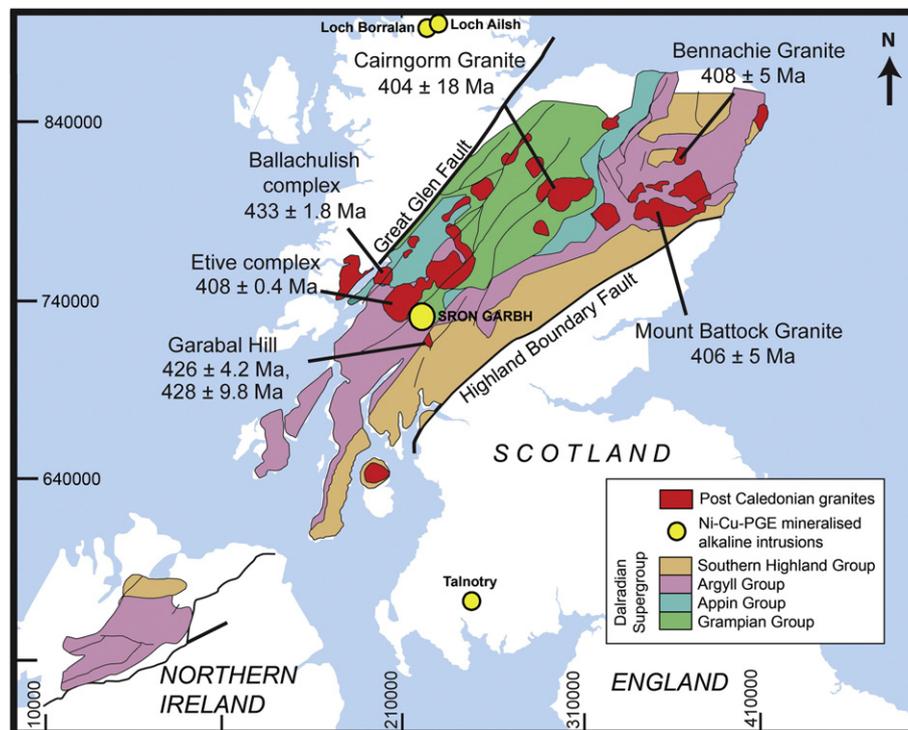
Fig. 1. Simplified regional geological map of Scotland and Northern Ireland showing the post-Caledonian intrusives, the Dalradian Supergroup and Cu-Ni-PGE-Au mineralised alkaline intrusions. The Grampian terrane lies between the Highland Boundary Fault and the Great Glen Fault. Dates for post-collisional intrusives are taken from; Conliffe et al. (2010); Neilson et al. (2009); Oliver et al. (2008).
Adapted from Hill et al. (2013).

tectonic stacking and metamorphism between 490 and 465 Ma (Stephenson et al., 2013). Subduction of oceanic lithosphere is believed to have ceased c. 430 Ma (Neilson et al., 2009) and by c. 423 Ma orthogonal shortening had switched to sinistral transpression (Stone, 1995) along NE-SW trending faults parallel to the Highland Boundary and Great Glen faults that bound the Grampian Terrane. Within this terrane the Dalradian Supergroup hosts the three largest Au resources in the UK at Curraghinalt and Cavanacaw in Northern Ireland, and at Cononish, near Tyndrum in Scotland (Fig. 2; Dalradian Resources, 2012; Galantas Gold Corporation, 2013; Tanner, 2012; Hill et al., 2013).

2.1. Post collision magmatism

Post-collision calc-alkaline granitic and appinitic intrusions are widespread throughout the Grampian Terrane (Fig.1). The granodiorite-granite suites were emplaced over a c. 25 Ma period and are often spatially and temporally associated with appinites (Stephenson and Gould, 1995; Neilson et al., 2009; Conliffe et al., 2010). They are dominated by a high Ba-Sr geochemical signature, distinct from I, S and A-type granites through having low Rb, high K/Rb, low Th, U and Nb, low Y, high Ba and Sr, high Ni, Cr and MgO (Tarney and Jones, 1994; Fowler et al., 2001; Neilson et al., 2009).

The Ballachulish Complex (Fig. 1) is the oldest post-collisional granite emplaced at 433 ± 1.8 Ma (Re-Os molybdenite; Conliffe et al., 2010). Numerous other intrusives were dated by Oliver et al. (2008), such as the Cairngorm Granite, the Bennachie Granite and the Mount Battock granite (Fig. 1) which provide ages between 404 Ma and 408 Ma. In the Tyndrum area, there are no outcrops of granite present; however a gravity low that extends from the Etive Complex into the Tyndrum area is believed to be an undercover extension of the granite at Etive (Pattrick et al., 1988). Garabal Hill (Fig. 1), Glen Fyne, Arrochar and Rubha Mor appinites located approximately 40 km south of Sron Garbh were dated by U-Pb titanite and zircon to be ~426 to 428 Ma (Rogers and Dunning, 1991; Neilson et al., 2009).

This regional magmatism is thought to be linked to the earlier subduction of oceanic crust beneath Laurentia causing metasomatism of the mantle wedge (Fowler and Henney, 1996; Fowler et al., 2001). The subsequent hydrous partial melting post-collision is ascribed to an uplift-decompression event (~15–20 km) following the orogeny that enables mantle melting (Halliday and Stephens, 1984) although some authors postulate a slab-drop off event produced the magmatism (Atherton and Ghani, 2002; Neilson et al., 2009).

2.2. Appinites

The appinite intrusions in the Grampian Terrane are a group of ultramafic-intermediate composition rocks (e.g. Fowler and Henney, 1996 and references therein). They are spatially and temporally associated with the post collisional granite intrusions. They are usually found as stocks, dykes and sheets located in or proximal to the granites (Hamidullah, 2007). The most distinctive and typical rock type of the suite is a coarse, hornblende-rich meladiorite that is usually porphyritic with phenocrysts of brown-green amphibole within a groundmass with equal proportions of plagioclase and orthoclase feldspar. The appinite suite also includes cortlandite (hornblende peridotites), kentallenite (phlogopite bearing picrites), hornblendites, and hornblende gabbros (e.g. Hamidullah, 2007). The most evolved members of the suite are leucocratic granodiorites, rare examples of biotite-rich granites and a large variety of felsic segregations, globular structures and veins containing varying proportions of orthoclase, plagioclase, quartz and carbonate all occurring in irregular masses (Fowler and Henney, 1996). Evidence of multiple intrusions, magmatic and hydrothermal remobilisation, in situ differentiation, and complex country rock interactions is common (Fowler and Henney, 1996).

3. Geology and mineralisation of the Tyndrum area

Located 2 km north of Tyndrum (Fig. 2), Sron Garbh is situated on the eastern section of the Orchy Dome, between the Ericht-Laidon and Tyndrum Faults (Tanner and Thomas, 2009). The Beinn Udlaidh massif is composed of the upper part of the Dalradian Grampian Group (Meall Garbh Psammite) and the lowermost section of Appin Group (Lochaber Subgroup) (Fig. 2). Four phases of deformation occurred during the Grampian Event with peak amphibolite grade metamorphism (Oliver, 2001; Tanner and Thomas, 2009). The Orchy Dome comprises a series of isoclinal, SE-facing recumbent folds and is intruded by numerous irregular shaped sills, dykes, and minor intrusions, the majority of which are vogesites, similar to Sron Garbh (Tanner and Thomas, 2009). Tanner and Thomas (2009) outline that the intrusions were emplaced into the pre-formed Orchy Dome and are commonly located along margins of the Beinn Udlaidh Quartzite (Fig. 2), locally linked to dykes, and observed to pass outwards into sills from the larger irregular shaped intrusions. The Sron Garbh intrusion was emplaced into the Meall Garbh Psammite Formation (MGP) (Fig. 2). The 1000 m thick MGP is a flaggy, finely banded to laminated psammite, semi-pelite and pelite, with lateral variation and a transitional upper boundary (10s m) with the Beinn Udlaidh Quartzite Formation (Tanner and Thomas, 2009).

The Tyndrum area contains an abundance of hydrothermal Au mineralisation (Fig. 2) of controversial origin (Hill et al., 2013) that post-dates the appinites. The Cononish quartz vein is the largest and is currently owned by Scotgold Resources (Treagus et al., 1999; Tanner, 2012; Hill et al., 2013). Other notable gold occurrences are at Halliday's Veins (Pattrick et al., 1988), and the Beinn Udlaidh Main Vein (Tanner, 2012). There is also an abundance of base-metal sulfide (BMS) mineralisation that is younger than the gold veins. This was historically mined at the Tyndrum Lead Mine (Pattrick et al., 1988).

4. Samples and methods

Field mapping and logging of drill core from Sron Garbh was undertaken on Scotgold Resources' exploration licence areas during 2012. Four AQ (3 cm diameter) drill cores that intersected the full range of rock types around Sron Garbh identified by field mapping were logged and sampled: SGAQ33, 35, 36 and 37. A total of 26 samples were collected, representative of all rock types and mineralisation styles; 22 from drill core, and 4 as grab samples (Fig. 3).

All 26 samples were analysed for bulk rock geochemistry by XRF using the PANalytical Axios-Advanced XRF spectrometer, operating with PANalytical SuperQ software at the University of Leicester. Trace elements were determined from pressed powder pellets and major element analysis was carried out on fused glass beads created with 0.6 g of ignited powder and ~3 g of 80% lithium metaborate-20% tetraborate flux. Whole-rock S concentrations were determined by standard combustion iodometric procedures using a Laboratory Equipment Company (LECO) titrator at the University of Leicester. Depending on the sulfide content between 0.05 and 0.2 g of sample was combusted for each titration. The standard deviations of wt% S determined from triplicates ranged from 0.005 to 0.016. Scotgold Resources provided geochemical datasets for 16 drill holes (SGAQ 13–29). These analyses were carried out by ALS Geochemistry, Ireland, by four acid, ICP-MS and ICP-AES analysis (ME-MS61), producing a dataset of 48 elements. Standard Pt, Pd and Au assay was carried out by fire assay and ICP-AES finish from a 30 g sample (PGM-ICP23). Four full PGE (Pt, Pd, Rh, Ru, Ir, Os) and Au analyses were undertaken using 30 g samples by fire assay with nickel sulfide collection and neutron activation analysis (PGM-NAA26).
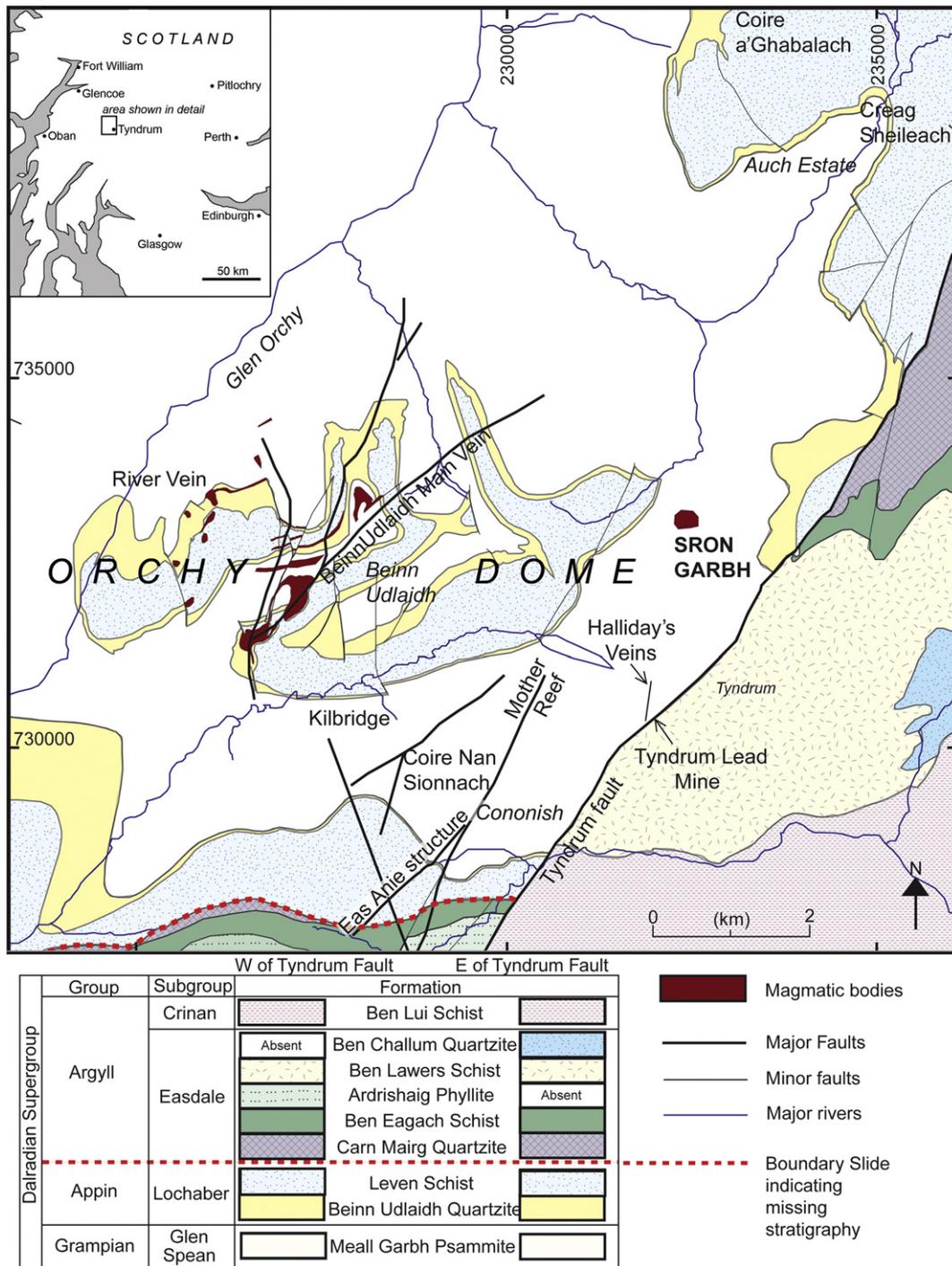
Fig. 2. Local geological map of the Tyndrum/Glen Orchy area showing the Orchy Dome, local Caledonian intrusives and Sron Garbh. After Hill et al. (2013).

Mineralogical identification of platinum group minerals (PGM) was done on six polished thin sections at the University of Leicester using a Hitachi S-3600N Environmental Scanning Electron Microscope, coupled to an Oxford Instruments INCA 350 energy dispersive X-ray analysis system. Further investigation was carried out at the Carl Zeiss Natural Resources Laboratory, Cambridge, using a ZEISS SIGMA VP coupled with Bruker 6│30 energy dispersive spectrometers.

In situ sulfide analyses were carried out using a New Wave Research UP213 UV laser system coupled to a Thermo X Series 2 ICP-MS at Cardiff

University. The relative abundances of PGE and other elements were recorded in time-resolved analyses mode (time slices of 250 ms) as the laser beam followed a line designed to sample different sulfide phases. The beam diameter employed was 30 μm, with a frequency of 10 Hz and a power of ~6 J cm^{-2}. The sample was moved at 6 μm s^{-1} relative to the laser along a predetermined line pattern. Ablations were carried out under He (flow, ~0.7 L min^{-1}), and the resulting vapour combined with Ar (flow rate, 0.65–0.75 L min^{-1}) before delivery to the ICP-MS. Acquisitions lasted between 80 and 400 s, including a 20 s gas blank
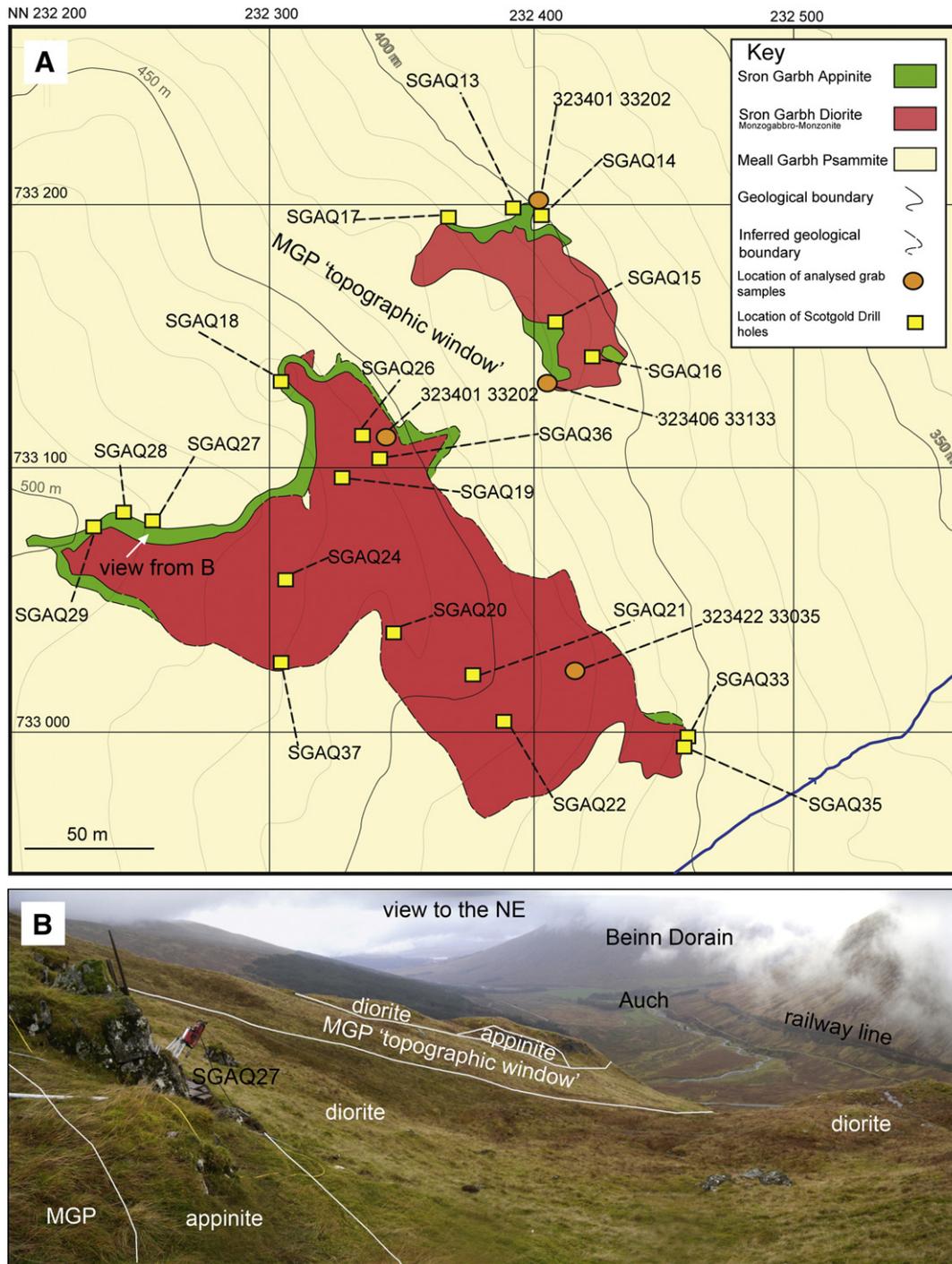
Fig. 3. A: Geological map of Sron Garbh with locations of sampling and drilling. A topographic depression (the MGP 'topographic window') separates the intrusion to create two outcrops; B: photograph of the Sron Garbh intrusion looking NE from the site of drill hole SGAQ27. The railway is the Glasgow to Fort William line.

prior to the start of the analysis and a 10 s washout at the end. Signals in the time spectra that could be attributed to PGM included in the sulfides were not selected for integration so the data reflect concentrations in the sulfide minerals alone. Sulfur concentrations were measured prior to laser ablation (LA)-ICP-MS using the electron microprobe at the University of Leicester and ^{33}S was used as internal standard. Subtraction of gas blanks and internal standard corrections were performed using Thermo Plasmalab software. Calibration was performed using a series of five synthetic Ni-Fe-S standards prepared from quenched sulfides. The standards incorporate S, Ni, Fe and Cu as major elements and Co, Zn, As, Se, Ru, Rh, Pd, Ag, Cd, Sb, Te, Re, Os, Ir, Pt, Au and Bi as trace

elements and the compositions of the five standards, and discussion of necessary argide corrections are given in Prichard et al. (2013) and Smith et al. (2014).

Eighteen S isotope analyses were carried out at the Scottish Universities Environmental Research Centre (SUERC) at East Kilbride, Scotland. Conventional analysis was carried out with 5–10 mg of micro-drilled powdered sulfide sample following the standard combustion with cuprous oxide technique of Robinson and Kusakabe (1975). Liberated SO_2 was analysed using a VG Isotech SIRA II mass spectrometer with standard corrections applied to raw $\delta^{66}SO_2$ to produce true $\delta^{34}S$. International standards NBS-123 and IAEA-S-3 and internal SUERC standards

CP-1 were used. Repeat analyses gave δ^{34}S values of $+17.1‰$, $-31.5‰$ and $-4.6‰$ respectively with a standard error of $<0.2‰$. When grains were <1 mm in size in situ laser combustion of sulfides was carried out on polished blocks using the technique outlined in Kelley and Fallick (1990) and Wagner et al. (2002). Correction factors are applied as a result of fractionation of δ^{34}S following laser combustion (Wagner et al., 2002). Correction factors were established and applied by SUERC with 0.8 and 0.7 applied to pyrite and chalcopyrite respectively. Reproducibility for laser combustion is identical to conventional analysis at $\pm 0.2‰$ (Wagner et al., 2002).

5. Field relationships of the Sron Garbh intrusion

Our detailed mapping of the Sron Garbh intrusion (Fig. 3A) shows two separate outcrops of appinite-diorite rocks, intruded into the Meall Garbh Psammite (MGP), with a slight topographic depression between the two. The two outcrops of igneous rock are in a prominent topographic bulge on the western hillside of Glen Orchy (Fig. 3B). Both outcrops are dominantly monzodiorite-monzonite (Sron Garbh diorite) with a distinctive and irregular appinite rim, up to a few metres in thickness. Both the appinite and the diorite are in contact with the MGP, although there are no clear exposures that demonstrate the dip of the contact between the intrusion and the country rocks. As such, it is unclear from the exposures present (and the lack of deep drilling) whether the appinite forms a rim around two pipe-like bodies of diorite, or a basal few metres of a sill roughly parallel with the slope of the hillside; either of which would be consistent with the exposure of the appinite-diorite suite in two topographic bulges.

The diorite is largely homogenous and dominated by orthoclase, plagioclase, quartz and biotite. The appinite rim is heterogeneous, containing abundant amphibole phenocrysts that often display cumulate textures and layers (Fig. 4A). The amphiboles, when associated with
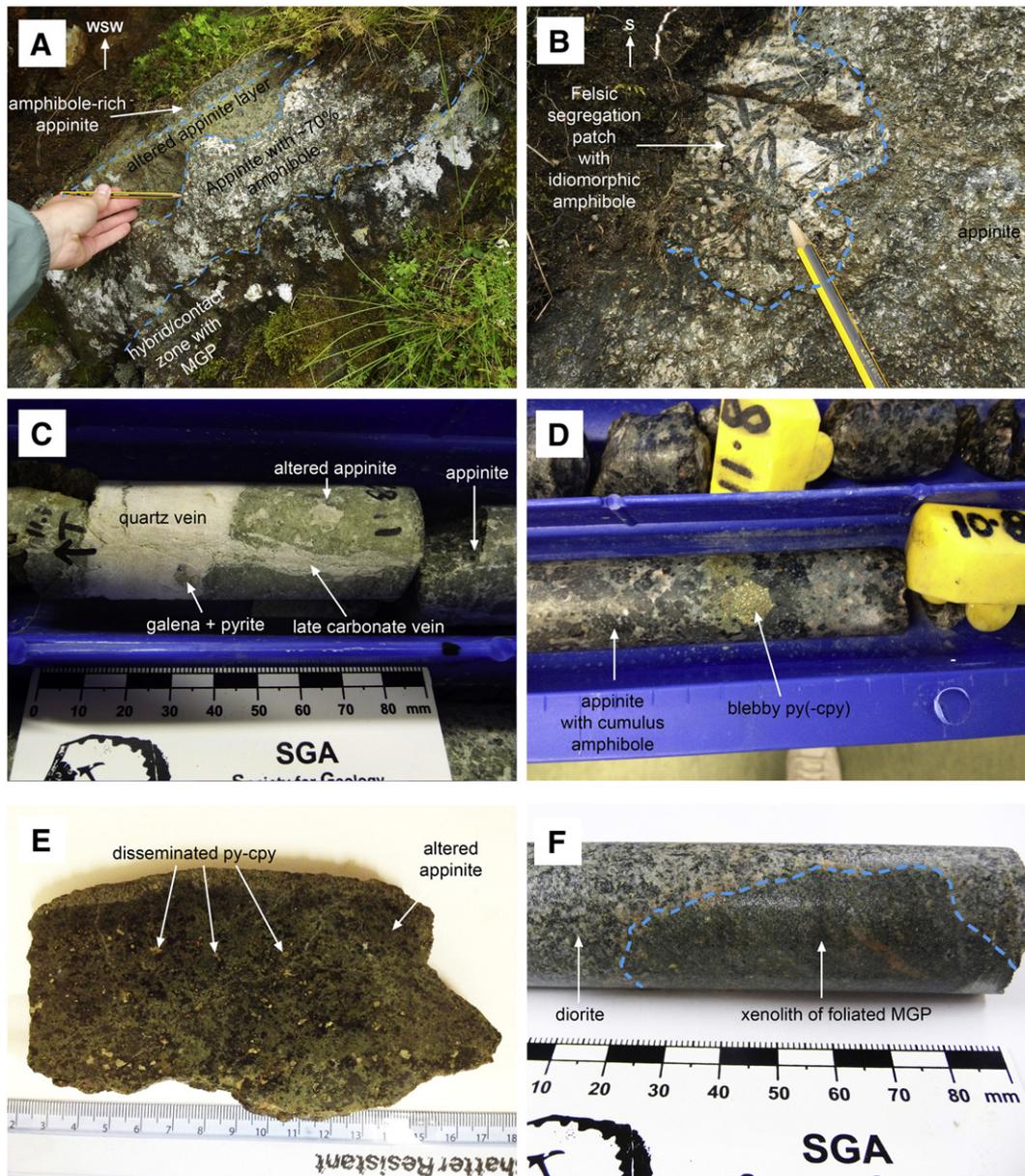
Fig. 4. Field and core photographs showing key geological relationships: A: amphibole-rich appinite cumulate layers with the contact with psammite (MGP) observed below at GR32414 33047; B: idiomorphic amphibole crystals concentrated within the felsic segregations observed at GR 32311 32988; C: pyrite and galena bearing quartz vein cutting the Sron Garbh intrusion; D: blebby pyrite-chalcopyrite mineralisation located within the appinite; E: disseminated, PGE-bearing chalcopyrite (cpy) and pyrite (py) mineralisation in appinite; F: partially digested MGP xenoliths in the diorite.

the felsic blebs are idiomorphic and coarse, suggesting that volatiles were concentrated in the felsic segregations during cooling and crystallisation (Fig. 4B). The intrusion is cross cut by a series of quartz veins that contain some galena and pyrite (Fig. 4C). The style of sulfide mineralisation in the appinite is variable between a coarse blebby assemblage of pyrite and chalcopyrite (Fig. 4D) and a more disseminated texture with a similar sulfide assemblage (Fig. 4E). Xenoliths of the country rock MGP are found in almost exclusively in the more felsic rich diorite and evidence of diorite inclusions in the appinite are also present (Fig. 4F).

6. Petrology

6.1. Appinite

The appinite is a vari-textured, usually porphyritic, amphibole rich (25–85 modal %) rock, containing orthoclase, plagioclase, phlogopite, quartz, and primary calcite. Classification of the rocks under lamprophyre nomenclature is as vogesites, based on the dominant amphibole phase and greater proportion of orthoclase over plagioclase (Rock, 1984). The amphibole phenocrysts are hornblendes up to 1 cm in size, typically idiomorphic-xenomorphic and produce mesocumulate-orthocumulate textures (Fig. 5A–D). The groundmass also contains abundant hornblende aggregates which are idiomorphic-xenomorphic and up to 1 mm in size (Fig. 5B).

Alteration of the hornblende is variable with examples of minor to complete alteration by secondary amphibole (actinolite-tremolite), secondary calcite, chlorite and sericite (Fig. 5C). Some amphibole phenocrysts contain chalcopyrite and pyrite inclusions (Fig. 5C). Orthoclase is an intercumulus phase (Fig. 5A), sometimes as globular myrmekitic intergrowths with quartz (Fig. 5B). Minor amounts of phlogopite are present along with primary calcite, interstitial to the amphibole phenocrysts (Fig. 5D). Plagioclase and quartz are relatively minor accessory phases and the majority of the quartz is located in the myrmekite graphic intergrowths (Fig. 5B).

6.2. Diorites

The Sron Garbh diorite is relatively homogenous, consisting of orthoclase, plagioclase, quartz, biotite, calcite and accessory phases of pyrite, titanomagnetite, zircon and apatite. The most abundant phase is orthoclase (up to 40 modal %) and regularly shows myrmekite intergrowths (Fig. 5E). The orthoclase is partly to completely replaced, and often turbid with sericitized cores and a combination of sericite, calcite and chlorite replacement. Alteration of the myrmekite leaves isolated island of quartz surrounded by the alteration assemblage. Plagioclase is either as an accessory phase or up to 25 modal % of the sample with idiomorphic laths that are labradorite to anorthite in composition and dominantly altered by sericite, minor calcite and rare examples of chlorite. Biotite (up to 50 modal %) forms idiomorphic laths that are strongly
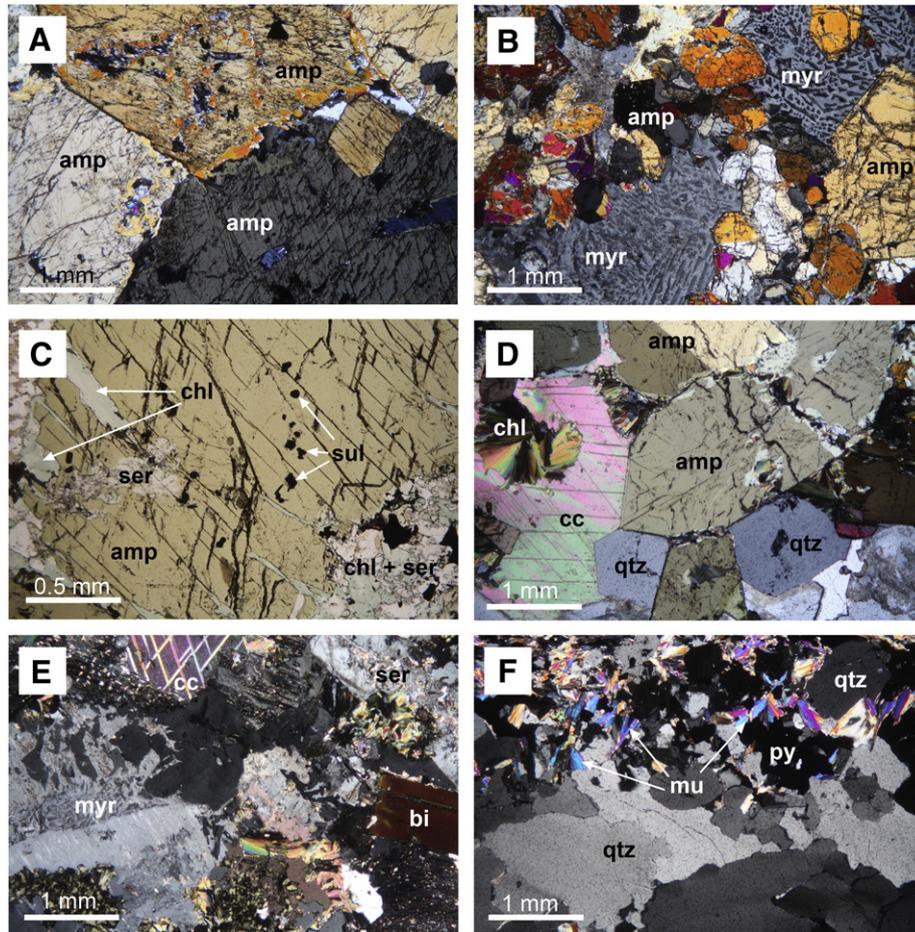
Fig. 5. Photomicrographs showing examples of the textures observed in the appinite (A–D), the diorite (E) and the MGP (F). All images in cross-polarised light except C, which is plane polarised light. A: example of amphibole (amp) orthocumulates with minor interstitial material; B: typical groundmass assemblage of mesocumulate appinite with amphibole aggregates and an example of the myrmekite (myr) intergrowths of quartz and feldspar; C: large amphibole phenocryst with alteration by sericite (ser) and chlorite (chl) and inclusions of sulfide (sul); D: example of primary, interstitial calcite (cc) and quartz (qtz) within appinite; E: diorite with myrmekitic intergrowths of quartz and feldspar and biotite (bi) phenocrysts; F: psammite with layers of pure quartz, and layers with abundant muscovite (mu) and pyrite (py).

Table 1
Bulk rock geochemical data from the 22 drill core samples and 4 grab samples from the Sron Garbh appinite, diorite and MGP formation. All data obtained by XRF, except S, which was determined by LECO. Rock types: App = appinite, SGD = Sron Garbh Diorite, MGP = Meall Garbh Psammite.

Sample	10.6	8.4	9.1	9.69	10.8	12.22	13.33-13.2	14.63	323406 33133	32405 33086	1.06	22.97	0.5	4.53	6.09
Rock type	App	App	App	App	App	App	App	App	App	App	SGD	SGD	SGD	SGD	SGD
Drill hole	33	35	35	35	35	35	35	37	Grab	Grab	33	33	35	35	35
SiO_2	51.87	52.50	53.36	50.96	48.97	50.23	48.77	43.76	49.19	43.23	47.87	49.27	56.02	55.31	53.32
TiO_2	0.82	0.51	0.42	0.59	1.07	0.83	1.15	1.42	0.41	0.73	1.00	0.56	0.69	0.92	0.82
Al_2O_3	11.16	8.55	6.84	8.77	10.22	10.56	13.03	10.62	4.79	10.69	14.90	9.49	16.10	14.82	13.98
Fe_2O_3	10.33	6.83	6.75	7.94	9.45	10.37	10.30	11.15	8.49	8.32	7.92	6.10	4.90	7.59	6.34
MnO	0.133	0.125	0.139	0.154	0.152	0.153	0.152	0.129	0.152	0.158	0.133	0.160	0.086	0.111	0.103
MgO	7.77	12.02	12.25	10.74	12.78	8.70	8.34	14.44	16.32	9.19	4.51	7.74	2.82	4.38	4.36
CaO	9.13	10.85	14.55	11.28	11.44	9.41	8.72	11.06	15.85	8.34	6.67	11.71	5.58	4.96	4.63
Na_2O	2.07	1.42	1.19	1.57	1.70	1.71	2.12	1.55	0.42	0.17	2.99	1.37	3.01	2.99	2.70
K_2O	1.873	1.798	1.544	1.945	1.725	2.056	2.184	1.377	0.389	2.150	3.508	1.740	3.457	3.368	3.390
P_2O_5	0.164	0.118	0.061	0.077	0.097	0.130	0.312	0.056	0.052	0.254	0.287	0.109	0.185	0.123	0.064
SO_3	2.045	0.128	0.331	0.471	0.405	2.441	0.316	0.835	0.807	0.380	1.579	0.041	0.105	<0.002	0.017
CrO_3	0.044	0.166	0.089	0.074	0.123	0.075	0.016	0.105	0.221	0.080	0.004	0.128	0.001	0.003	0.004
NiO	0.036	0.015	0.028	0.024	0.026	0.020	0.003	0.036	0.065	0.030	<0.0003	0.003	<0.0003	<0.0003	<0.0003
LOI	2.53	5.03	2.67	4.52	1.62	2.75	3.81	3.53	2.77	14.47	8.15	10.34	6.53	5.33	4.74
Total	99.97	100.06	100.22	99.12	99.78	99.44	99.22	100.06	99.94	98.20	99.53	98.76	99.50	99.91	94.47
S wt%															
As ppm	1.6	4.0	4.3	9.9	4.0	6.5	1.9	21.2	97.7	0.2	0.4	1.0	8.5	6.9	1.4
Ba ppm	453.5	462.5	609.9	455.5	424.9	672.4	585.2	426.7	522.6	111.6	763.0	363.4	1141.2	1294.2	937.8
Co ppm	39.0	45.1	48.4	69.1	47.7	40.5	41.3	66.6	38.9	60.8	18.4	24.8	12.7	23.8	21.0
Cu ppm	45.3	168.7	169.3	599.5	116.7	779.2	127.9	196.4	23.7	1821.6	7.9	10.6	7.1	17.7	42.8
Cr ppm	1265.2	659.2	524.3	346.3	923.5	587.6	125.7	774.2	535.5	1674.4	30.6	1035.9	13.6	26.5	46.9
Ni ppm	143.1	230.2	197.7	284.3	232.4	151.1	44.2	312.2	238.1	481.3	11.5	47.1	3.8	8.7	10.8
Pb ppm	9.2	4.1	5.9	9.0	4.3	6.4	6.1	4.0	23.2	4.9	10.8	12.8	16.3	11.0	14.9
Rb ppm	40.4	31.8	50.4	38.5	28.4	43.1	49.3	79.2	55.5	9.8	76.8	51.5	75.2	74.2	22.8
Sr ppm	359.7	415.4	313.6	459.6	336.2	364.1	478.2	509.3	647.8	120.2	450.9	383.2	433.2	519.9	655.3
Zn ppm	48.0	42.1	57.0	53.8	63.4	64.6	69.9	56.4	156.5	55.2	75.1	59.1	45.5	66.7	53.7
Zr ppm	102.1	66.0	83.1	117.8	61.3	80.5	97.1	117.8	119.7	36.3	186.4	104.6	668.2	79.4	368.1
Y ppm	14.2	12.6	16.2	22.3	24.1	21.7	26.5	20.1	20.7	14.8	26.6	19.8	33.2	20.3	24.6

associated with titanomagnetite laths (Fig. 5E). Pyrite is present as a ubiquitous disseminated phase made up of aggregates of subhedral-euhedral grains up to 3 mm in size, but more commonly ~1 mm. Alteration of the biotite is mainly by chlorite with observed pseudomorphing of the laths with minor amounts of calcite and sericite. Primary calcite is present which is overprinted by secondary sericite and chlorite.

6.3. Host rock metasediments

The host rock MGP is a medium grained quartz dominated (>90 modal %) psammite that contains accessory muscovite mica, some clays and rare, disseminated pyrite (Fig. 5F).

7. Bulk rock geochemistry

Bulk rock XRF analyses of selected grab samples and drill core are shown in Table 1. Major element bivariate diagrams demonstrate the element variation between the appinite and diorite (Fig. 6). The appinites have higher MgO and CaO (Fig. 6A, C) and lower Al_2O_3 and K_2O (Fig. 6D, E) than the diorites which reflect the amphibole and calcite content of the appinites, and the feldspar and biotite contents of the dioites. The Fe_2O_3 is generally higher in the appinites, though the diorites have a much larger range (Fig. 6B), which is likely to be controlled by the presence of variable amounts of pyrite. The TiO_2 contents of the suites overlap (Fig. 6F) but may be due to the presence of Ti in the amphibole in the appinite and in biotite and titanomagnetite in the diorite.

Fig. 7A shows a multi-element chondrite normalised diagram from drill hole SGAQ 14 (Table A1), which sampled a representative section through the diorite into the appinite cumulate and provides a direct comparison between the two units from a continuous section. Both the appinite and the diorite have comparable trace element profiles, with the diorite more enriched in all elements consistent with it being a more fractionated variant of the appinite. The moderate enrichment

in LILE and a negative Nb-Ta anomaly usually interpreted as characteristic of subduction-related magmatism (e.g. Saunders et al., 1988; McCulloch and Gamble, 1991) and the negative P anomaly highlights the calc-alkaline nature of the suite and its incompatibility in the appinite mafic cumulate.

Fig. 7B shows the relationship between Ba and Cr to further outline the trend from appinite to diorite. Barium is readily substituted into feldspar and biotite, which are abundant in the diorite, whereas Cr substitutes into amphibole. The data outline two clusters, which represent the two suites; the appinite suite with high Cr (amphibole segregation) and low Ba (low feldspar and biotite abundance); the diorite contains low Cr (no amphibole) and high Ba (abundant feldspars and biotite). The two suites are distinct indicating two separate magmas, but ones that have a similar affinity, with the diorite being a more fractionated version of the appinite (Fig. 7A). The rare occurrences of overlap are attributed to cross-boundary sampling.

8. Mineralisation

The base and precious metal sulfide mineralisation at Sron Garbh is found solely in the appinitic portions of the intrusion. Bulk rock grades are up to 0.92 wt% Cu, 0.27 wt% Ni (Table 3) and 0.91 ppm Pt, 0.81 ppm Pd and 0.63 ppm Au (Table 4). The Sron Garbh diorite contains some disseminated, typically euhedral-subhedral, pyrite up to 1 cm in size, which can comprise up to 5 modal % of the rock. However this unit does not contain any base or precious metal mineralisation.

8.1. Base metal sulfide assemblages

The mineralisation in the Sron Garbh appinite can be split into two textural types: (1) a blebby pyrite-chalcopyrite assemblage (Fig. 4D); and (2) a disseminated chalcopyrite-pyrite assemblage (Fig. 4E) more common in the most mafic (amphibole-rich) appinites. Both styles

Sample	14.17-14.14	15.06-14.93	16-15.88	7.02-6.77	7.52-7.38	25.13	32345 33113	32422 33035	17.04	17.62	20.3
Rock type	SGD	SGD	SGD	SGD	SGD	SGD	SGD	SGD	PM MGP	MGP	MGP
Drill hole	35	35	35	35	35	36	Grab	Grab	35	37	37
SiO_2	52.52	49.45	53.55	54.76	58.27	44.60	53.73	48.39	58.23	59.33	60.03
TiO_2	0.80	1.13	0.61	0.72	0.76	0.86	0.87	1.09	0.78	0.85	1.00
Al_2O_3	15.67	14.98	16.21	14.03	15.04	15.09	14.95	15.41	14.55	15.96	17.43
Fe_2O_3	9.46	8.76	6.76	5.36	5.83	7.04	7.87	10.09	7.03	6.60	5.50
MnO	0.105	0.120	0.102	0.094	0.087	0.178	0.113	0.147	0.094	0.117	0.057
MgO	3.29	5.22	1.92	3.70	4.48	2.03	3.71	3.44	2.07	2.07	1.70
CaO	5.63	6.90	5.46	4.69	3.99	10.86	5.23	5.96	2.46	2.54	1.51
Na_2O	3.06	2.41	2.88	3.46	3.23	3.15	4.70	1.08	2.32	2.55	0.09
K_2O	2.489	3.068	3.518	2.727	3.218	3.096	1.173	3.881	3.353	3.685	5.462
P_2O_5	0.311	0.141	0.207	0.062	0.136	0.291	0.252	0.400	0.267	0.206	0.092
SO_3	0.749	0.182	1.230	0.064	0.048	4.120	0.609	3.098	0.968	0.296	0.252
CrO_3	0.003	0.004	0.000	0.003	0.003	0.002	0.000	0.001	0.004	0.002	0.005
NiO	<0.0003	<0.0003	<0.0003	<0.0003	<0.0003	<0.0003	<0.0003	<0.0003	<0.0003	<0.0003	<0.0003
LOI	5.86	6.61	5.52	5.71	5.10	7.77	5.47	6.80	4.37	4.78	6.19
Total	99.94	98.98	97.97	95.38	100.19	99.09	98.69	99.79	96.49	98.98	99.31
S wt%									0.56	0.15	0.15
As ppm	1.4	2.2	1.2	2.0	1.8	0.9	1.7	16.1	3.2	0.4	32.1
Ba ppm	882.0	779.8	1186.6	928.7	1073.2	991.7	499.6	848.0	929.6	725.9	954.9
Co ppm	36.4	28.0	15.5	17.4	19.0	13.6	18.0	19.0	18.4	15.8	11.4
Cu ppm	197.8	12.4	22.3	41.4	41.3	15.8	27.6	25.4	33.4	36.0	5.8
Cr ppm	25.2	27.7	12.4	36.9	31.0	22.3	3.6	16.2	51.2	30.7	42.5
Ni ppm	20.0	5.9	6.6	10.4	13.9	3.7	3.8	3.2	24.1	18.7	16.4
Pb ppm	12.4	5.5	12.1	13.4	12.2	4.6	10.7	9.9	22.8	14.8	9.5
Rb ppm	61.3	86.8	103.9	48.9	65.6	72.4	112.0	119.9	29.8	160.7	224.6
Sr ppm	582.4	877.5	714.5	549.7	431.0	349.5	359.5	270.3	354.2	239.2	68.6
Zn ppm	70.0	74.0	65.1	48.2	52.4	48.0	67.8	97.1	90.7	89.8	46.8
Zr ppm	84.3	74.6	162.4	90.4	136.7	108.2	247.0	149.5	54.4	224.8	447.5
Y ppm	19.3	22.6	20.6	18.9	19.0	24.4	37.9	30.1	22.5	45.4	43.3

contain minor millerite and Ni-Co-As-sulfides and no pentlandite, reflecting the Cu-rich and Ni-poor nature of the sulfide assemblage.

8.1.1. Blebby sulfides

This mineralisation style is most prominent and features irregular blebs of sulfide up to 3 cm in size, located sporadically throughout the more felsic parts of the appinite (Fig. 4D). The blebs are made up predominantly of pyrite (~80%) that contains some chalcopyrite (~20%) as a series of cross cutting veins/slivers and isolated inclusions (Fig. 8A, B), and rims around the edges of the pyrite (Fig. 8B). Nickel is present in minor sulfides include millerite (NiS) bravoite ((Fe, Ni)S_2), hengleinite ((Ni, Fe, Co)S_2), gersdorffite (NiAsS) and cobalt-nickel pyrite ((Co, Ni)S_2). The Ni-bearing sulfides are rare and found at pyrite-chalcopyrite grain boundaries, as inclusions and as exsolved rims around other sulfides.

8.1.2. Disseminated sulfides

The disseminated pyrite-chalcopyrite assemblage is distributed sporadically throughout the more amphibole-rich parts of the appinite (Fig. 4E). The sulfides are part of the interstitial assemblage and are observed to pool alongside and embay silicates (Fig. 8C). Furthermore, they are found as inclusions within amphiboles and less commonly the myrmekite intergrowths. This assemblage is more chalcopyrite-rich (~35, but up to 70 modal % of the sulfide assemblage; Fig. 8D) and Ni-Co sulfides are more common (~10 modal % of the sulfide assemblage). The pyrite is sporadically disseminated, xenomorphic with idiomorphic occurrences, <5 mm in size (Fig. 8C–E). Textural relationships between the pyrite and chalcopyrite are variable with examples of pyrite hosting chalcopyrite, disseminated chalcopyrite surrounding the edge of pyrite but most commonly idiomorphic pyrite with amorphous and chalcopyrite (Fig. 8D, E). Pyrite in this assemblage is generally more euhedral

than in the blebby style. Alteration of sulfides is by secondary amphiboles such as tremolite-actinolite (Fig. 8D). The Ni-Co-As-sulfides form a minor assemblage of millerite, hengleinite, bravoite, vaesite (NiS$_2$), cobaltite (CoAsS), gersdorffite and cobalt-nickel pyrite that are intergrown with and exsolved from pyrite and chalcopyrite (Fig. 8F).

8.2. Platinum-group mineralogy

Sixty nine individual platinum-group minerals (PGM) grains were identified and are listed in Table 2. Each individual grain has been classified by its composition, size and association. Grain sizes as a volume were calculated assuming an ellipsoid around the short- and long-axes of PGM. To prevent biases, we present all data on PGM assemblages in percentage of total volume of all PGM, which reflects more accurately the relative proportions of each PGM type within an assemblage.

Six separate PGM types were identified and the typical textures and associations are outlined in Fig. 9. Platinum-group minerals were found almost exclusively in the disseminated chalcopyrite-pyrite mineralisation style. The PGM assemblage is dominated by the bismutho-sulfide malyshevite (PdCuBiS$_3$; Fig. 9A) and the telluride kotulskite (Pd(Te,Bi); Fig. 9B–D) which make up 75% by volume of the total PGM assemblage (Fig. 10A). Significantly, Pd-bearing PGM represent the vast majority (90%) of the total PGM by volume, with the remaining 10% Pt-bearing PGM, of which 99.6% by volume were sperrylite (PtAs$_2$) together with a single grain of cooperite (PtS).

The PGM associations (by number of grains) are made up roughly equally of inclusions in sulfides, sulfide-silicate grain boundaries, and inclusions in silicates (Figs. 9B, 10). For those PGM associated with sulfide, there is a strong preference to be located in, or next to chalcopyrite
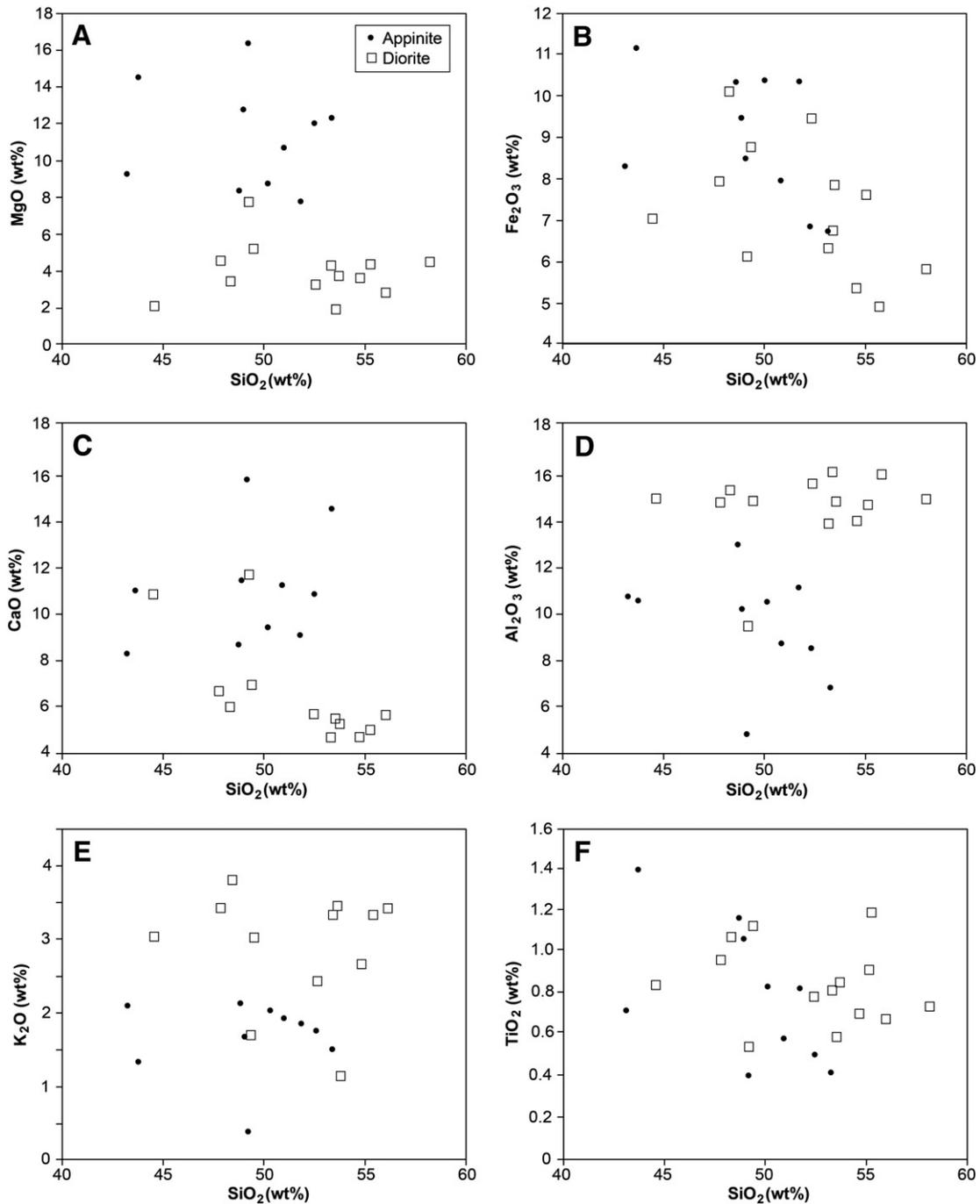
Fig. 6. Major element bivariate plots from XRF analysis of samples from the appinite and the diorite (data in Table 1).

(Figs. 9, 10B). The PGM included in silicate are located very close to sulfides, and chalcopyrite in particular (Fig. 8B).

8.3. Precious, base and semi metal geochemistry

The geochemistry from 21 mineralised samples ('mineralised' defined as having Pt + Pd > 50 ppb; Table 3) from Scotgold's assay database are shown in Fig. 11. These data are from appinites from the drill program around Sron Garbh, as shown in Fig. 2. Samples are mostly 0.5–1 m in length and thus can contain examples of both styles of mineralisation (blebby and disseminated) which are distributed sporadically on a scale of tens of centimetres. Therefore, this geochemical data can be considered as being representative of the appinite as a

whole. That said, the observation of PGM in the disseminated sulfides would imply that appreciable grades of PGE in the rocks equate to the presence of the disseminated style.

The data show that Pt and Pd correlate very well throughout the appinites (Fig. 11A). The PGE and Au abundances also show positive, but slightly variable correlations with Ni and Cu (Fig. 11B, C, D) and are thus sulfide controlled, but with some variability in respective ratios, possibly due to sampling of variable proportions of the two sulfide styles. The correlation between Pd and Cu (Fig. 11B) is consistent with the observed PGM association with chalcopyrite (Fig. 9). Copper is dominant over Ni, with Cu/Ni ratios for the mineralised rocks around 3 (Fig. 11E; Table 3). The good correlation between Cu and Ni (Fig. 11E), indicates most of the bulk Ni in mineralised samples

Fig. 7. Bulk rock geochemistry for appinite and diorite portions of the Sron Garbh intrusion. A: Chondrite normalised trace element profiles; B: Ba vs. Cr.

peak at either Au, or Pd, as the Sron Garbh data shows as well. The Sron Garbh samples are more Cu and Ni rich, but the precious metal profiles are very similar.

The bulk rock Pt/Pd ratio of 0.83 (Fig. 11A; Table 3) is inconsistent with the observations presented in the PGM analysis, which identified 90% by volume of all PGM to be Pd phases. Thus, there is a mass balance problem that indicates some Pt to be present in minerals other than the PGM. Given the well-defined correlations shown in Fig. 11, Pt appears to be controlled by sulfide and thus if it is not present as PGM associated with the sulfides, and is therefore likely to be present as a trace element in the sulfides themselves.

8.4. PGE concentrations of base metal sulfides

The results of a series of LA-ICP-MS analyses of sulfide minerals (chalcopyrite, pyrite, millerite and a Co-Ni-Fe-sulfide, hengleinite) from the Sron Garbh appinite are listed in Table 5. Time-resolved analysis (TRA) spectra of a representative number of these are shown in Fig. 13. The analyses were performed along lines across the surface of the sections, as shown in the inset images in Fig. 13, and thus the TRA spectra show the progression of the laser across different mineral phases.

8.4.1. Chalcopyrite

All chalcopyrite analyses are from disseminated blebs as shown in the inset images in Fig. 13. The trace element compositions are highly consistent, containing means of around 150 ppm Se, 110 ppm Ag and 3 ppm Bi (Table 5). No significant PGE or Au concentrations were found in any of the chalcopyrite analyses, and where Pt is present at up to 1.4 ppm, it coincided with elevated Te and/or Bi contents and most likely represents microinclusions of PGM in the analysis. The smooth, parallel TRA profiles (Fig. 13A, B, E, F) for all chalcopyrite analyses indicate no zonation, and the presence of Se and Ag in solid solution.

8.4.2. Pyrite

Two textural forms of pyrite were analysed: blebby (e.g. Figs. 8A, B, 13C); and euhedral grains that form part of the disseminated chalcopyrite-rich style (e.g. Figs. 8E, 13A, D, E). The blebby pyrite has generally higher Co and As contents by close to an order of magnitude, and slightly lower Se contents (mean of 159 compared to 187) than the disseminated pyrite (Table 5). Both generations, however, contain variable concentrations of Pt, up to 22 ppm in one analysis of blebby pyrite, which is shown in Fig. 13C. The smooth, consistent profile of the Pt signal on the TRA profile indicates Pt in solid solution in the pyrite. The euhedral pyrite shows strong zonation towards the outer edges, shown in a number of the TRA spectra. Fig. 13A shows that Co and Pt drop from a plateau towards the edge of the grain, whereas Fig. 13D shows a complete traverse through a pyrite where Co, As and Pt are enriched at the margins. Fig. 13E also shows that Pt is present in the outer portion of the grain, with concurrent increases in Se and Ni.

8.4.3. Millerite

Millerite is present in some of the disseminated grains along with chalcopyrite, and Fig. 13B shows a laser analysis through chalcopyrite, millerite, then a mixed millerite-chalcopyrite signal before entering chalcopyrite. The millerite portion shows consistent Ni, Co, Ag, Bi and Se signatures, along with some detectable Au and Pd (Fig. 13F; Table 5). Millerite is the only sulfide to contain Au, with concentrations up to 0.5 ppm and also has the highest concentrations of Bi (mean: 34 ppm) and Se (mean: 267 ppm; Table 5).

is held in sulfide, presumably in the minor millerite and Co-Ni-As-sulfides. However, the drop off in Cu/Ni ratio is the least mineralised samples is probably a result of some Ni in silicate, whereas Cu can reasonable be assumed to be in sulfide. Cobalt, however, shows more scatter with Ni (Fig. 11F), and given the good Ni-Cu correlation, this may indicate Co is present heterogeneously in other phases, such as pyrite. The S and Se contents of the rocks are variable compared with the base metal concentrations due to the presence of varying proportions of the two mineralisation styles present in any one sample (Table 3). This can be seen in Fig. 11G–I, which show the relationship between Cu, Ni and Co relative to Se (a good proxy for S). All show a positive relationship, again indicating Cu, Ni and Co are hosted by sulfides, but there is more scatter than the very well constrained Pt-Pd relationship, for example, indicating the presence of the two sulfide populations within individual samples. However, all samples have S/Se ratios in the range 3289–7788 (Table 3), within and above the established mantle range of 2850–4350 (Eckstrand and Hulbert, 1987) and above the mantle mean of ~3250 (e.g. Lorand et al., 2003), indicating contribution from crustal S in all samples as crustal rocks have S/Se ratios higher than the mantle range, <100,000 (Yamamoto, 1976).

The primitive mantle normalised PGE, Au, Cu and Ni data from four samples selected from the high grade appinite ore (Table 4; Fig. 12) show a strongly fractionated pattern with a depletion in the IPGE (Os, Ir, Ru), including a prominent negative Ru anomaly, and an enrichment of Pt, Pd and Au with a mean Pd/Ir ratio of 108 (Table 4; Fig. 12). For comparison, data for the mineralisation in the Mordor Alkaline Igneous Complex, Australia (Barnes et al., 2008) is also shown. This shows a very similar, steep, fractionated pattern, with a negative Ru anomaly, and a

Fig. 8. Sulfide mineralogy of the two styles of mineralisation. A, B, D and E are reflected light images. A and B: blebby pyrite (py) with inclusions and fracture fills of chalcopyrite (cpy), with minor chalcopyrite in the silicates surrounding the pyrite; C: plane polarised light photomicrograph of disseminated sulfide bleb of pyrite with some ingress into cumulus amphibole (amp) crystals; D: disseminated chalcopyrite and minor pyrite altered by secondary amphiboles (sec amp); E: euhedral pyrite grain as part of a disseminated sulfide bleb mostly composed of chalcopyrite. Note the laser ablation lines (c.f. Fig. 13); F: Backscattered electron image of Ni-Co-bearing sulfides violarite (vi) and gersdorffite (ger) associated with disseminated pyrite and chalcopyrite blebs.

8.4.4. Co-Ni-Fe-sulfide

One grain of a Co-Ni-Fe sulfide (hengleinite) contained very high concentrations of Se (768 ppm), and Te (19 ppm); plus Pt (1.1 ppm), Pd (2.2 ppm) and Bi (5.2 ppm) in solid solution (Fig. 13F).

In summary, Pt is hosted in solid solution by blebby pyrite (though in variable concentrations); zoned, euhedral pyrite; and by Co-Ni-Fe sulfide. Some Pd is also found in the Co-Ni-Fe sulfide and in millerite, which is the only host to Au in solid solution. Due to the variable concentrations of PGE within the sulfides, it is not possible to perform a robust mass balance calculation. However, the Pt concentrations of a few ppm can account for some of the bulk rock Pt that is not observed in the PGM assemblage.

9. S-isotopes

Eighteen S-isotope analyses from representative samples of the appinite, the diorite and the MGP are shown in Table 6 and Fig. 14 with regional S isotope data from Lowry (1991); Lowry et al. (1995) and Hill et al. (2013). The appinite samples produce a range of $\delta^{34}S$ values from +1.0 to +4.2‰ for pyrite (n. 11) and a single chalcopyrite value of +3.3‰ (Fig. 14) with an overall mean of +2.8‰. The range of values sit at the upper end, and above, the mantle range of 0 ± 3‰ (Ohmoto and Rye, 1979), though the more recent values for mantle $\delta^{34}S$ of -1.28 ± 0.33‰ (Labidi et al., 2013) would place all of the Sron Garbh data above mantle values and thus provide an indication

of the incorporation of isotopically heavy crustal S, which is consistent with the high S/Se ratios (Table 3). The Sron Garbh sulfides fit within, but at the upper end of the range for appinites in the region (Fig. 14). The diorite pyrite $\delta^{34}S$ values are distinctly higher, with a range of +3.9‰ to +4.8‰ (mean: +4.3‰, n. 4). Two analyses of pyrite from the immediate country rock MGP have $\delta^{34}S$ values that are higher still, at +4.9‰ and +5.3‰. The variation in the $\delta^{34}S$ value in each grouping has no correlation with the textural relationship of the sulfides (Table 5). Sulfides in the cross cutting quartz veins are isotopically heavier than the appinite, but are consistent with other veins in the area (Hill et al., 2013).

10. Discussion

The results of this work provide a number of newly recognised constraints on the nature and genesis of Cu-Ni-PGE-Au sulfide mineralisation in appinitic intrusions in Scotland, including: (1) geochemical and petrological evidence for the nature and origin of the appinite-diorite suite at Sron Garbh; (2) the mineralogical and geochemical characteristics of the sulfide mineralisation; and (3) the role of crustal contamination in the genesis of sulfide mineralisation. From this, we are able to produce a genetic model for the development of mineralisation in the Sron Garbh intrusion, and assess the wider implications for generating PGE mineralisation in lamprophyric intrusions worldwide.

Table 2
List of all named PGM with ideal formulae, their volumes (assuming an ellipsoid around the X (longest) and Y (perpendicular) axes, with Z = Y) and associations. All PGM located in samples 323401 and 323406. Abbreviations: sul = sulfide, sil = silicate, cpy = chalcopyrite, py = pyrite.

Name	Ideal formula	Type	Volume (µm³)	Association
Cooperite	PtS	Pt sulfide	0.79	Inclusion in py
Keithconnite	Pd₃Te	Pd-telluride	0.39	sul/sul grain boundary
Keithconnite	Pd₃Te	Pd-telluride	1.60	Inclusion in py
Kotulskite	Pd(TeBi)	Pd-telluride	224.62	cpy vein in py
Kotulskite	Pd(Te,Bi)	Pd-telluride	87.96	Inclusion in silicate
Kotulskite	Pd(Te,Bi)	Pd-telluride	25.27	Inclusion in silicate
Kotulskite	Pd(Te,Bi)	Pd-telluride	17.56	Inclusion in silicate
Kotulskite	Pd(Te,Bi)	Pd-telluride	7.07	Inclusion in silicate
Kotulskite	Pd(Te,Bi)	Pd-telluride	9.42	Inclusion in silicate
Kotulskite	Pd(Te,Bi)	Pd-telluride	54.98	Inclusion in silicate
Kotulskite	Pd(Te,Bi)	Pd-telluride	10.60	Inclusion in pyrite
Kotulskite	Pd(Te,Bi)	Pd-telluride	3.53	Inclusion in pyrite
Kotulskite	Pd(Te,Bi)	Pd-telluride	0.20	Inclusion in pyrite
Kotulskite	Pd(Te,Bi)	Pd-telluride	8.01	Inclusion in pyrite
Malyshevite	PdCuBiS₃	Pd-bismuthosulfide	131.95	cpy/sil grain boundary
Malyshevite	PdCuBiS₃	Pd-bismuthosulfide	452.39	cpy/sil grain boundary
Malyshevite	PdCuBiS₃	Pd-bismuthosulfide	31.42	cpy/sil grain boundary
Malyshevite	PdCuBiS₃	Pd-bismuthosulfide	82.47	cpy/sil grain boundary
Malyshevite	PdCuBiS₃	Pd-bismuthosulfide	47.12	cpy/sil grain boundary
Malyshevite	PdCuBiS₃	Pd-bismuthosulfide	39.27	cpy/sil grain boundary
Malyshevite	PdCuBiS₃	Pd-bismuthosulfide	12.57	cpy vein in py
Malyshevite	PdCuBiS₃	Pd-bismuthosulfide	9.42	cpy vein in py
Malyshevite	PdCuBiS₃	Pd-bismuthosulfide	26.51	cpy vein in py
Malyshevite	PdCuBiS₃	Pd-bismuthosulfide	0.79	sul/sul grain boundary
Malyshevite	PdCuBiS₃	Pd-bismuthosulfide	30.16	sul/sul grain boundary
Malyshevite	PdCuBiS₃	Pd-bismuthosulfide	2.36	sul/sul grain boundary
Malyshevite	PdCuBiS₃	Pd-bismuthosulfide	11.78	sul/sul grain boundary
Malyshevite	PdCuBiS₃	Pd-bismuthosulfide	1.37	Inclusion in cpy
Malyshevite	PdCuBiS₃	Pd-bismuthosulfide	49.48	Inclusion in cpy
Malyshevite	PdCuBiS₃	Pd-bismuthosulfide	14.53	Inclusion in cpy
Malyshevite	PdCuBiS₃	Pd-bismuthosulfide	5.50	Inclusion in py
Malyshevite	PdCuBiS₃	Pd-bismuthosulfide	6.28	Inclusion in py
Merenskyite	Pd(Te,Bi)₂	Pd-telluride	0.79	Inclusion in silicate
Mertieite II	Pd₈(Sb,As)₃	Pd antimonide	8.64	sul/sil grain boundary
Mertieite II	Pd₈(Sb,As)₃	Pd antimonide	0.79	sul/sil grain boundary
Mertieite II	Pd₈(Sb,As)₃	Pd antimonide	2.75	sul/sil grain boundary
Mertieite II	Pd₈(Sb,As)₃	Pd antimonide	11.00	cpy vein in py
Naldrettite	Pd₂Sb	Pd antimonide	0.79	sul/sil grain boundary
Naldrettite	Pd₂Sb	Pd antimonide	2.67	sul/sil grain boundary
Naldrettite	Pd₂Sb	Pd antimonide	0.79	sul/sil grain boundary
Naldrettite	Pd₂Sb	Pd antimonide	3.93	sul/sil grain boundary
Naldrettite	Pd₂Sb	Pd antimonide	7.85	cpy vein in py
Naldrettite	Pd₂Sb	Pd antimonide	11.78	cpy vein in py
Naldrettite	Pd₂Sb	Pd antimonide	1.57	sul/sul grain boundary
Naldrettite	Pd₂Sb	Pd antimonide	2.59	Inclusion in silicate
Naldrettite	Pd₂Sb	Pd antimonide	1.57	Inclusion in silicate
Naldrettite	Pd₂Sb	Pd antimonide	6.28	Inclusion in silicate
Naldrettite	Pd₂Sb	Pd antimonide	4.56	Inclusion in silicate
Naldrettite	Pd₂Sb	Pd antimonide	61.26	Inclusion in silicate
Sobolevskite	Pd(Bi,Te)	Pd bismuthide	0.79	sul/sil grain boundary
Sobolevskite	Pd(Bi,Te)	Pd bismuthide	9.42	Inclusion in cpy
Sobolevskite	Pd(Bi,Te)	Pd bismuthide	7.85	sul/sil grain boundary
Sobolevskite	Pd(Bi,Te)	Pd bismuthide	98.96	sul/sul grain boundary
Sobolevskite	Pd(Bi,Te)	Pd bismuthide	9.42	Inclusion in silicate
Sobolevskite	Pd(Bi,Te)	Pd bismuthide	3.93	Inclusion in silicate
Sobolevskite	Pd(Bi,Te)	Pd bismuthide	3.14	Inclusion in silicate
Sobolevskite	Pd(Bi,Te)	Pd bismuthide	9.42	Inclusion in silicate
Sperrylite	PtAs₂	Pt arsenide	8.25	sul/sil grain boundary

Table 2 (continued)

Name	Ideal formula	Type	Volume (µm³)	Association
Sperrylite	PtAs₂	Pt arsenide	0.79	Inclusion in silicate
Sperrylite	PtAs₂	Pt arsenide	133.52	Inclusion in silicate
Sperrylite	PtAs₂	Pt arsenide	0.79	Inclusion in silicate
Sperrylite	PtAs₂	Pt arsenide	1.18	Inclusion in silicate
Sperrylite	PtAs₂	Pt arsenide	9.42	Inclusion in cpy
Sperrylite	PtAs₂	Pt arsenide	0.79	Inclusion in cpy
Sperrylite	PtAs₂	Pt arsenide	3.93	Inclusion in cpy
Sperrylite	PtAs₂	Pt arsenide	2.36	Inclusion in cpy
Sperrylite	PtAs₂	Pt arsenide	1.57	Inclusion in cpy
Sperrylite	PtAs₂	Pt arsenide	0.39	Inclusion in py
Sperrylite	PtAs₂	Pt arsenide	25.27	Inclusion in silicate

10.1. Classification and petrogenesis of the Sron Garbh intrusion

The post-collisional intrusive rocks in western Scotland (Argyll and Northern Highlands suites) are dominated by a high Ba-Sr (HiBaSr) geochemical signature (Tarney and Jones, 1994; Fowler et al., 2001; Neilson et al., 2009). Barium and Sr data for the Sron Garbh appinite-diorite suite is plotted along with other HiBaSr intrusions from Scotland and China in Fig. 15. There is a clear similarity in Ba-Sr ratio between Sron Garbh and the other intrusions, and the Sron Garbh rocks are comparable in terms of Ba and Sr contents with the lower range of Scottish HiBaSr rocks and are similar to the appinite-granite suites reported in Tibet by Ye et al. (2008). Neilson et al. (2009) reported a fairly constant Sr/Ba ratio of 1.2 for the appinites they sampled, and our data is similar to this, giving a range of 0.5 to 1.2, with a mean of 0.9 (from Table 1).

The HiBaSr magmatic sub-class is interpreted to be a result of a slab-break off or delamination event (Atherton and Ghani, 2002; Ye et al., 2008; Neilson et al., 2009), with a combination of hydrous mantle melting from slab dehydration, partial melting of subducting slab and melting of subducted sediments all enriching the melt/wedge and contributing to the distinctive geochemical signature. The source of some of the high Ba and Sr has been attributed to pelagic clays and carbonate sediments, respectively, which are then metasomatically enriched in the mantle wedge during prolonged subduction (Plank and Langmuir, 1998; Zanetti et al., 1999). Asthenospheric upwelling into the space created by the slab drop off enables melting of the enriched mantle wedge, generating a basaltic-lamprophyric underplate (Atherton and Ghani, 2002; Fowler et al., 2008). This under-plating is responsible for the widespread HiBaSr granitic emplacement from the fractionation of basic-lamprophyric melts (Fowler et al., 2008) or, more likely, widespread partial melting of mafic-intermediate lower crust (Neilson et al., 2009).

Some constraints on the depth of emplacement of Sron Garbh can be gained from fluid inclusion studies on the mineralised quartz veins in the area, which cross cut Sron Garbh (Fig. 4F). Curtis et al. (1993) and Pattrick et al. (1988) provide emplacement depths of the Cononish and Halliday's quartz veins (Fig. 2) at between 3 and 4 km. Fluid inclusions from the nearby Beinn Udlaidh breccia pipes which cross cut lamprophyres on Beinn Udlaidh (Fig. 2) provide depths of 2.9–5.9 km from CO_2 inclusions, and ~3.5 km for H_2O-CO_2-NaCl inclusions (Moore, 2011). Assuming the veins that cross cut Beinn Udlaidh are equivalent to those that cut Sron Garbh, these data would impose an emplacement depth for Sron Garbh of at least 3–4 km.

10.2. Genesis of sulfide mineralisation in the Sron Garbh intrusion

Sron Garbh is a very small intrusion, but yet the sulfides that are present contain significantly elevated PGE contents, indicating
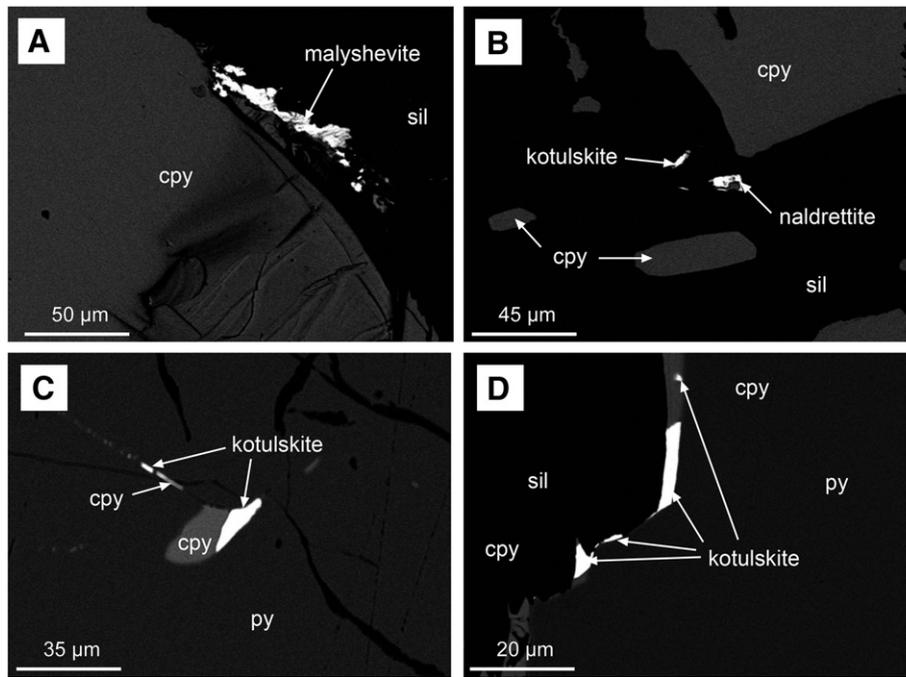
Fig. 9. Typical associations of PGM in the disseminated ores showing a strong affiliation with chalcopyrite. A: large malyshevite grain at the boundary between chalcopyrite (cpy) and silicate (sil); B: grains of kotulskite and naldrettite included in silicate, but within a few tens of microns of chalcopyrite; C: kotulskite intimately associated with chalcopyrite as an inclusion in pyrite (py); D: kotulskite with chalcopyrite located along the margin of a pyrite grain.
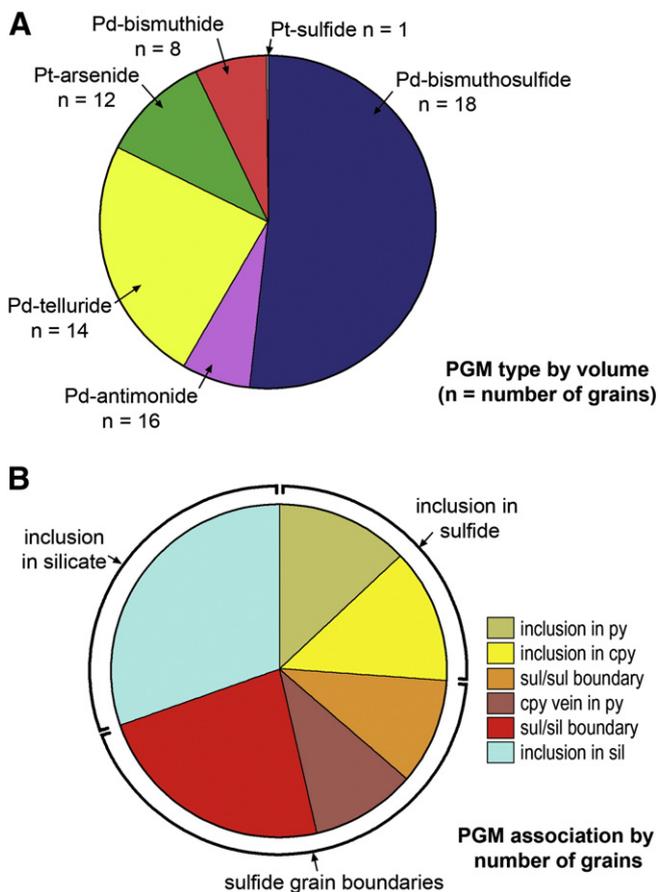
Fig. 10. A: relative proportion of PGM types by volume. Total number of grains (n) also shown; B: PGM associations by number of grain from a total of 69 PGM.

interaction with appreciable amounts of magma (Naldrett, 2011). As such, it is unlikely that sulfide saturation took place in situ, and transport of sulfides from a larger magma source, or interaction with magma in a conduit is likely to have taken place (e.g. Barnes et al., 2016). Sulfide inclusions within amphibole phenocrysts (Fig. 6D) indicate the presence of an immiscible sulfide liquid during amphibole formation. Thus, it is likely that the trigger for sulfide saturation took place elsewhere in the magmatic plumbing system, most likely at depth, with sulfides brought up. That said, the identification of downward sulfide injection in some conduit systems highlights the possibility of ore genesis actually taking place at higher levels, with subsequent sulfide slumping (Barnes et al., 2016; Hughes et al., 2016).

The addition of crustal S by assimilation is widely accepted to be one of the most important and effective mechanisms of inducing sulfide saturation in magmas, and producing large, economic magmatic Ni-Cu-PGE deposits (e.g. Lesher et al., 1984; Li et al., 2002; Keays and Lightfoot, 2010). At Sron Garbh, the sulfides have S-isotope and S/Se ratio signatures that are indicative of some crustal input of S (Fig. 14). Comparisons of the Sron Garbh data with the data from Hill et al. (2013; Fig. 14) shows the diverse range of S-isotope values from mineralisation and intrusions in the Tyndrum area. However, the appinite and granitic bodies in the area all tend to have heavier $\delta^{34}S$ value than typical uncontaminated mantle-derived melts. Hill et al. (2013) attribute the $\delta^{34}S$ values of the later quartz-Au vein mineralisation in the area to the mixing of S from sedimentary and magmatic sources, and proposed that underlying SEDEX and VMS horizons in the Easdale Subgroup of the Argyll Group may have been a significant source of the S.

The pyrite-bearing MGP country rock that is present in direct contact with the Sron Garbh intrusion contains pyrite with $\delta^{34}S$ values around +5‰ (Fig. 14, Table 5), and represents a possible, traceable contaminant that could account for the $\delta^{34}S$ values in the magmatic rocks. The extent of possible in situ crustal S addition can

Table 3
Precious and base metal, S and Se concentrations and ratios for a number of mineralised appinite (>50 ppb Pt + Pd) samples from Sron Garbh. na = not analysed.

Sample ID	Pt + Pd ppb	Pd ppb	Pt ppb	Au ppb	Co ppm	Cr ppm	Cu ppm	Ni ppm	S wt%	Se ppm	Pt/Pd	Cu/Ni	S/Se
SGAQ16-13	1568	794	774	275	91	531	9152	1720	2.50	7.60	0.82	5.32	3289
SGAQ15-07	1142	627	515	147	226	782	8841	2716	4.46	9.52	0.82	3.26	4684
SGAQ16-12	1137	756	381	159	132	829	5784	1800	2.49	6.21	0.76	3.21	4009
SGAQ14-13	973	563	410	185	276	885	6115	1602	5.82	9.32	0.73	3.82	6244
SGAQ26-23	675	307	368	109	378	789	6527	2124	6.50	12.5	0.81	3.07	5200
28AQ28-06	587	323	264	34	320	774	1619	1276	na	na	0.80	1.27	–
SGAQ15-06	544	302	243	32	101	882	3777	1023	1.82	3.05	0.82	3.69	5967
SGAQ18-11	250	146	104	7	54	886	1183	457	0.80	1.64	0.80	2.59	4878
SGAQ17-15	172	105	68	10	144	949	1529	1140	2.50	3.21	0.50	1.34	7788
SGAQ17-17	159	84	75	5	83	857	570	411	0.90	1.71	0.97	1.39	5263
SGAQ18-12	131	70	62	7	43	743	293	162	0.60	1.61	0.64	1.81	3726
SGAQ15-08	131	73	58	9	65	342	1302	450	0.57	1.55	0.89	2.89	3677
SGAQ14-12	130	74	56	6	46	881	711	342	0.32	<0.5	0.90	2.08	–
SGAQ18-10	91	45	46	7	75	751	975	277	1.00	1.39	0.84	3.51	7194
SGAQ17-18	78	41	37	5	70	523	529	218	1.30	1.71	1.04	2.43	7602
SGAQ14-02	76	42	34	2	46	578	184	95	0.65	<0.5	0.71	1.95	–
SGAQ28-12	69	36	33	82	66	642	203	454	na	na	0.89	0.45	–
SGAQ14-11	65	36	29	6	47	893	300	197	0.43	<0.5	1.20	1.52	–
SGAQ18-09	61	33	28	3	58	761	344	293	0.40	0.87	0.82	1.17	4597
SGAQ14-14	59	32	26	2	43	867	156	283	0.10	<0.5	0.74	0.55	–
SGAQ28-08	54	31	23	16	113	602	412	342	na	na	0.92	1.20	–

be modelled using a simple two component mixing model (Ripley and Li, 2003).

$$\delta^{34}S\,(\text{sulfide mixture}) = \frac{\delta^{34}S_c f_c C^s_c + \delta^{34}S_m f_m C^s_m}{f_c C^s_c + f_m C^s_m} \qquad (1)$$

where, f_c and f_m are fractional abundances of the contaminant and magma respectively and C^s is the concentration of S.

The S content for Caledonian appinites is not well known, so we use a typical C^s_m of 800 ppm for lamprophyres (Li et al., 2009), with a $\delta^{34}S$ value of +1‰ for the magma. For the contaminant, we use a C^s_c of 0.15 wt% (from Table 1) and a $\delta^{34}S$ of +5.1‰ (mean from Table 6). From these parameters, it would require ~19% contamination of the MGP to produce the +2.8‰ average value of the Sron Garbh appinite. Such large quantities of the MGP would be difficult to melt and would drastically alter the chemistry to very SiO₂-rich compositions, which is not observed. Also, this model works along the assumptions that there is only one contamination event (MGP as the source) and that the values we measured for the MGP are representative, which are all limiting assumptions, especially given the MGP is folded, and up to 1 km thick (Tanner and Thomas, 2009). The diorites are slightly, but distinctly isotopically heavier than the appinites (Fig. 14) and the presence of MGP xenoliths in the diorite may have allowed for more incorporation of MGP-sourced S to be assimilated into the diorites.

Thus the MGP is unlikely to have been the major source and trigger of sulfide saturation, at least not in situ. Hill et al. (2013) highlight that in the region there are various potential sources of S with high $\delta^{34}S$ present at depth (e.g. SEDEX deposits; Andersen et al., 2010; Stephenson et al., 2013) and that the thickness and repetition of the local stratigraphy at depth, due to recumbent folding, means that single stage modelling is unlikely to be appropriate. For the case of Sron Garbh, whereby the host magma presumably cut through this stratigraphy, this is highly pertinent, and, along with the unrealistic volume of contaminants needed from a simple two-component system, supports contamination at depth, from a number of possible sources.

10.3. The origin of the pyrite-chalcopyrite-dominant sulfide assemblages

We have identified two styles of sulfide in the Sron Garbh appinite: PGE-Au-bearing chalcopyrite-pyrite disseminations in the most amphibole-rich appinites, and pyrite-chalcopyrite blebs

in more felsic appinite. The mineralised rocks have a very Cu-dominant assemblage that differs from conventional magmatic sulfides that contain pentlandite-pyrrhotite-chalcopyrite(-pyrite). There is no pentlandite or pyrrhotite present and there are examples where pyrrhotite-pentlandite-chalcopyrite has undergone low temperature alteration/recrystallisation to form an assemblage of pyrite-chalcopyrite ± Ni-Co bearing sulfides (Dare et al., 2011; Djon and Barnes, 2012; Smith et al., 2014) at temperatures < 230 °C (Naldrett and Kullerud, 1967; Naldrett et al., 1967; Craig, 1973; Misra and Fleet, 1974). However, these are relatively rare and contain appreciable millerite after pentlandite. Furthermore, we observe inclusions of pyrite-chalcopyrite within relatively fresh hornblende (Fig. 5C) that would suggest it may be a primary assemblage. Thus, it should be considered that the Sron Garbh mineralisation may simply be a Cu-rich system and that the disseminated chalcopyrite-pyrite assemblage is a primary magmatic one. Pyrite can form directly from low temperature re-equilibration of a S-rich magmatic sulfide liquid (Naldrett et al., 1967). Sulfide saturation of a strongly fractionated mafic magma will produce a Cu-rich sulfide liquid, though this is known to produce bornite-dominant assemblages (Ripley et al., 2002). However, the nature of the magmas at Sron Garbh were not conventional ultramafic-mafic systems, being more volatile-rich, alkaline magmas. We suggest that the disseminated assemblage of chalcopyrite with euhedral pyrite, Ni-Co-As sulfides and PGM (Fig. 8D, E) may represent a primary assemblage formed from a Cu-PGE-rich sulfide liquid at relatively high fS₂ that allowed for pyrite, rather than pyrrhotite formation.

The key difference between this 'primary' sulfide style and the blebby style is the texture of the pyrite (Figs. 4D, 8A, B). These two styles may form a continuum, however, there does appear to be a host rock control and a compositional difference, with the Co and As contents of the blebby pyrite close to an order of magnitude higher than in the disseminated pyrite and Pt contents on average higher in the disseminated pyrite (Table 5), which may attest to a genetic distinction between the two. In a study of pyrite from the Great Dyke, Piña et al. (2016) identified two generations of pyrite: a euhedral, magmatic generation formed directly from low temperature decomposition of monosulfide solid solution; and a euhedral-subhedral generation interpreted to be formed via late stage hydrothermal replacement. Both Co and As concentrations are higher in the secondary, hydrothermal pyrite, and Pt contents are higher in the primary pyrite. This is consistent with the Sron Garbh
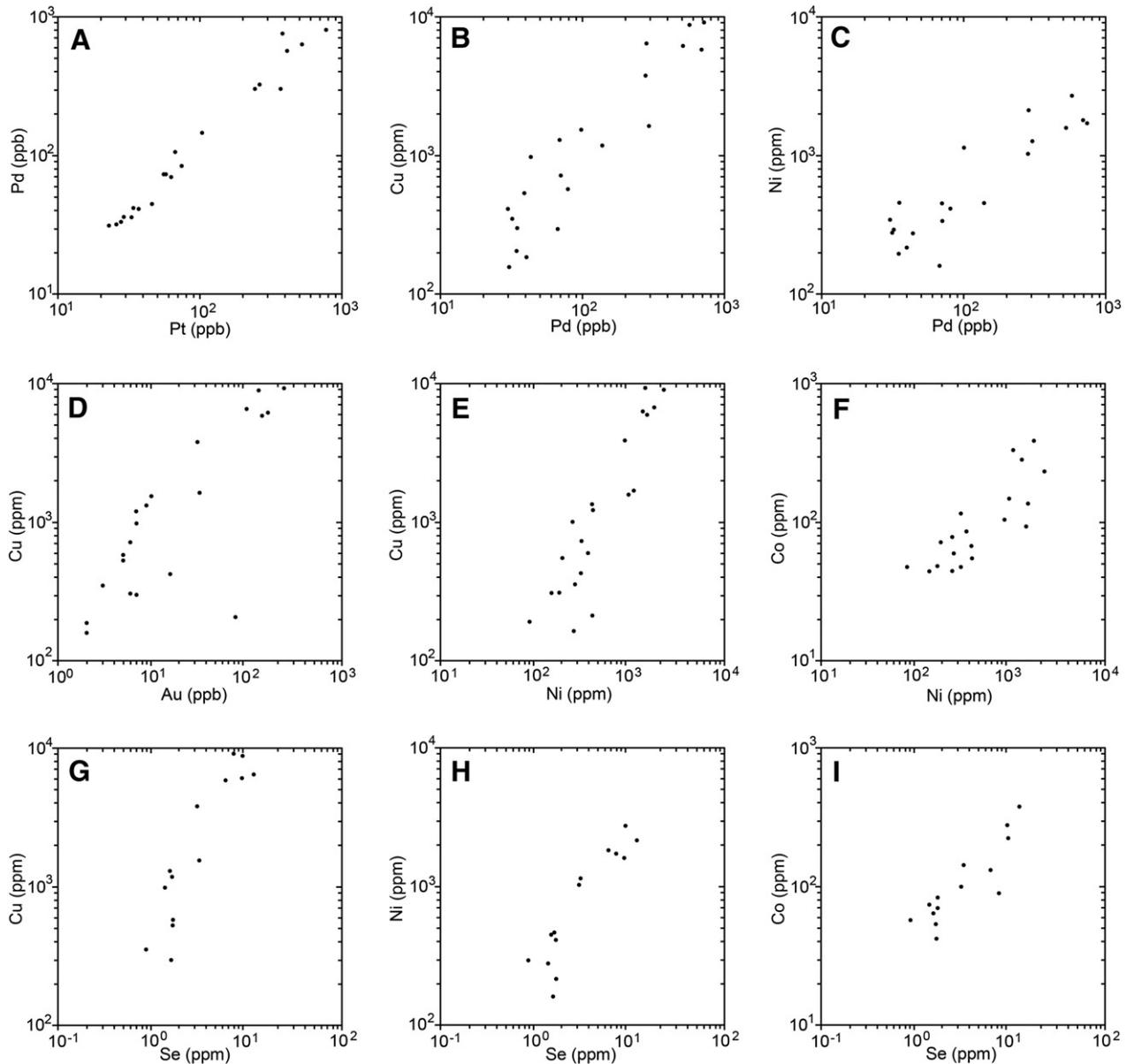
Fig. 11. Bivariate trace element plots of the PGE, base and semi-metal geochemistry using mineralised samples (>50 ppb Pt + Pd). A: Pd v Pt; B: Pd vs. Cu; C: Pd v Ni; D: Au v Cu; E: Ni v Cu; F: Ni v Co; G: Se v Cu; H: Se v Ni; I: Se v Co. Data from Table 3.

disseminated Pt-bearing assemblage being a primary magmatic one, and by comparison, the blebby Co-As-rich pyrite may have formed through late stage fluid interaction with an initially magmatic assemblage. The relatively poor correlation shown by Co and Ni in Fig. 11F is likely due to some samples having a higher proportion of this secondary, blebby pyrite, increasing the bulk Co concentration without a corresponding Ni increase.

The presence of pyrite aggregates throughout the appinite (as blebby sulfides) and also in the diorite may reflect a large scale secondary overprint of hydrothermal pyrite. Notably the S isotope data show that the diorite samples show slightly, though distinctly heavier $\delta^{34}S$ isotopic values, which would be consistent with formation from a hydrothermal fluid containing higher significant crustal. Quartz veins (related to the local gold and base

Table 4
Full PGE concentrations for samples of mineralised appinite.

Drill Hole	Depth	Os ppm	Ir ppm	Ru ppm	Rh ppm	Pt ppm	Pd ppm	Au ppm
SGAQ14-13	11.6–12.25	<0.01	0.013	<0.05	0.029	0.43	0.56	0.162
SGAQ15-07	5.5–6	<0.01	0.006	<0.05	0.016	0.69	0.57	0.632
SGAQ16-12	9.7–10.35	<0.01	0.004	<0.05	0.008	0.41	0.75	0.17
SGAQ16-13	10.35–11	<0.01	0.002	<0.05	0.007	0.91	0.81	0.414
Detection limits (ppm)		Os	Ir	Ru	Rh	Pt	Pd	Au
Upper		10	10	10	10	10	10	10
Lower		0.01	0.001	0.05	0.005	0.02	0.02	0.001
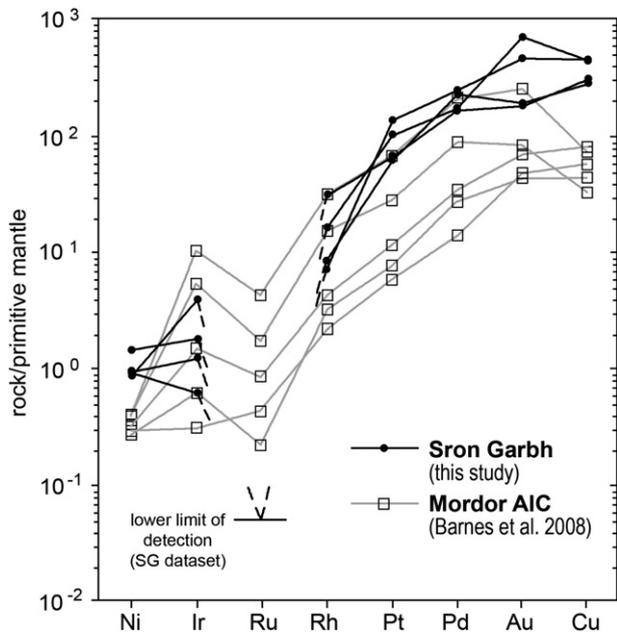
Fig. 12. Chondrite normalised PGE profile for Sron Garbh together with data for the Mordor Alkaline Igneous Complex, Australia (Barnes et al., 2008).

metal mineralisation) cross cut the Sron Garbh intrusion and could possibly be responsible for sulfidation of the intrusion, though the range is S isotope data for this hydrothermal episode (Hill et al., 2013) is too great to be able to use this as supporting evidence.

10.4. Concentration and mobilisation of precious, base and semi metals at Sron Garbh

The tight correlations shown in Fig. 11 indicate no significant variation between more and less mobile elements in the mineralised rocks. In particular, the lack of significant variation in Pt/Pd and Pt/Au ratios indicate that hydrothermal mobilisation is not significant, as this would decouple these elements and cause much greater scatter on cross-plots. Some hydrothermal alteration, however, has affected Sron Garbh, with chalcopyrite showing replacement by secondary silicates (Fig. 8D), as is common in many PGE sulfide deposits (e.g. Li et al., 2004). The PGM are overwhelmingly dominated by Te- and Bi-phases, which are considered to be characteristic of primary magmatic assemblages although the presence of Sb-bearing PGM (e.g. naldrettite; Table 2) is also highly characteristic of fluid affected assemblages (e.g. Holwell et al., 2006; Smith et al., 2014; Holwell et al., 2014). However, it has been shown in many cases that whilst this alteration may change the mineralogy, it is not significant in mobilising the PGE, although it can commonly decouple Cu and Au from PGE (e.g. Smith et al., 2014). Our geochemical data do not indicate such decoupling, and whilst the

Table 5
Laser ablation-ICP-MS analysis of sulfide minerals within the Sron Garbh appinite. bdl = below detection limit (which is indicated by <value). All Os, Ru and Ir values for all analyses were below detection limits and are thus not included in the table.

Sample	Texture	Mineral	57Fe %	59Co ppm	61Ni %	65Cu %	66Zn ppm	75As ppm	82Se ppm	103Rh ppm	106Pd ppm	109Ag ppm	111Cd ppm	125Te ppm	185Re ppm	195Pt ppm	197Au ppm	209Bi ppm
Memorial standard			63.12	<8	<0.02	<0.01	20	<15	<70	36.05	47.42	<0.8	<0.95	<1.3	<0.03	37.46	41.43	<0.05
SG1 An1	Dissem	cpy	23.90	<8	<0.02	29.66	<20	<15	122.3	<0.21	<0.14	121.0	<0.95	<1.3	<0.03	<0.02	<0.01	1.93
SG1 An1	Dissem	cpy	27.57	12.63	0.12	33.28	<20	<15	141.3	<0.21	<0.14	109.2	<0.95	<1.3	<0.03	<0.02	<0.01	0.88
SG1 An1	Dissem	cpy	25.02	<8	<0.02	29.36	<20	<15	129.9	<0.21	<0.14	97.15	<0.95	2.46	<0.03	<0.02	<0.01	0.61
SG1 An2	Dissem	cpy	22.17	10.36	<0.02	24.53	24.27	<15	107.6	<0.21	<0.14	99.82	<0.95	<1.3	<0.03	<0.02	0.03	1.59
SG2 An9	Dissem	cpy	29.51	<8	<0.02	34.22	<20	<15	155.0	<0.21	<0.14	118.9	<0.95	1.83	<0.03	<0.02	<0.01	1.95
SG2 An10	Dissem	cpy	28.92	41.17	0.05	30.17	<20	16.60	126.8	<0.21	<0.14	94.38	<0.95	2.77	0.03	0.64	0.03	4.05
SG2 An3	Dissem	cpy	30.15	27.14	0.03	32.70	<20	<15	141.1	<0.21	<0.14	124.8	<0.95	<1.3	<0.03	<0.02	0.04	3.61
SG2 An3	Dissem	cpy	27.81	29.01	<0.02	31.78	<20	<15	159.5	<0.21	<0.14	102.8	<0.95	<1.3	<0.03	<0.02	<0.01	3.18
SG32340 An6	Dissem	cpy	27.75	257.3	<0.02	28.50	<20	43.96	150.5	0.38	<0.14	104.9	<0.95	<1.3	<0.03	1.38	<0.01	1.77
SG32340 An4	Dissem	cpy	26.45	346.0	0.16	29.82	<20	<15	315.1	<0.21	<0.14	154.8	<0.95	2.22	<0.03	0.21	<0.01	12.92
Disseminated cpy		Mean[a]	26.93	73.6	0.04	30.40	11.43	12.06	154.9	0.13		112.8		1.32	0.02	0.23	0.01	3.25
		Max	30.15	346.0	0.16	34.22	24.27	43.96	315.1	0.38	bdl	154.8	bdl	2.77	0.03	1.38	0.04	12.92
		Min	22.17	bdl	bdl	24.53	bdl	bdl	107.6	bdl	bdl	94.38	bdl	bdl	bdl	bdl	bdl	0.61
SG1 An2	Blebby	py	46.96	416	0.23	0.06	<20	157.6	187.6	<0.21	28.35	6.70	<0.95	26.89	0.04	0.11	<0.01	17.90
SG32340 An6	Blebby	py	49.48	1251	0.11	0.04	<20	262.5	143.3	<0.21	<0.14	4.78	<0.95	<1.3	<0.03	2.51	<0.01	0.21
SG32340 An5	Blebby	Py	47.08	12,060	0.11	<0.01	<20	36.15	258.1	<0.21	<0.14	3.51	<0.95	<1.3	<0.03	<0.02	<0.01	0.19
SG323401 An9	Blebby	py	52.48	735	0.09	0.04	79.44	35.95	74.54	<0.21	<0.14	7.63	<0.95	<1.3	<0.03	<0.02	<0.01	0.83
SG323401 An9	Blebby	py	48.94	10,840	0.06	0.09	100.9	71.43	133.0	<0.21	<0.14	7.44	<0.95	<1.3	<0.03	21.74	<0.01	0.06
Blebby py		Mean[a]	48.99	5060	0.12	0.05	42.07	112.7	159.3		5.73	6.01		5.90	0.02	4.88		3.96
		Max	52.48	12,060	0.23	0.09	100.9	262.5	258.1	bdl	28.35	7.63	bdl	26.89	0.04	21.74	bdl	17.90
		Min	46.96	415.9	0.06	bdl	bdl	35.95	74.54	bdl	bdl	3.51	bdl	bdl	bdl	bdl	bdl	0.19
SG2 An9	Dissem	py	51.69	164.6	0.14	0.01	<20	20.50	71.86	<0.21	<0.14	<0.8	<0.95	<1.3	<0.03	0.17	<0.01	1.77
SG2 An10	Dissem	py	48.57	34.59	0.11	0.04	<20	16.96	90.46	<0.21	<0.14	1.25	<0.95	<1.3	<0.03	0.73	<0.01	2.64
SG2 An10	Dissem	py	49.36	8.21	0.50	0.01	<20	15.36	223.5	<0.21	<0.14	<0.8	<0.95	<1.3	<0.03	5.23	<0.01	0.59
SG2 An3	Dissem	py	49.84	253.6	0.21	0.06	24	30.32	255.6	0.27	<0.14	<0.8	<0.95	1.62	<0.03	1.09	<0.01	1.78
SG2 An3	Dissem	py	51.38	1126	0.29	<0.01	<20	20.27	297.6	0.23	<0.14	<0.8	<0.95	<1.3	<0.03	1.21	<0.01	1.38
Disseminated py		Mean[a]	50.17	317.4	0.25	0.03	12.72	20.68	187.8	0.16		0.57		1.62		0.84		1.63
		Max	51.69	1126	0.50	0.06	23.60	30.32	297.6	0.27	bdl	1.25	bdl	1.62	bdl	5.23	bdl	2.64
		Min	48.57	8.21	0.11	0.01	bdl	15.36	71.86	bdl	bdl	bdl	bdl	bdl	bdl	0.17	bdl	0.59
SG323401 An9	Dissem	mill	6.86	3293	49.41	8.61	38,900	<15	230.1	<0.21	0.84	62.84	2.89	<1.3	<0.03	<0.02	0.51	32.78
SG1 An1	Dissem	mill	1.62	4530	53.23	0.87	<20	16	304.1	0.26	12.68	502.9	1.10	<1.3	<0.03	<0.02	0.16	34.99
SG32340 An4	Dissem	Co-Ni-Fe-S	1.12	62,480	30.83	0.10	<20	<15	767.9	<0.21	2.21	9.64	<0.95	19.38	<0.03	1.12	<0.01	5.22

[a] Mean values include all data above detection limit. For values below the detection limit, 0.5 × detection limit was assumed.
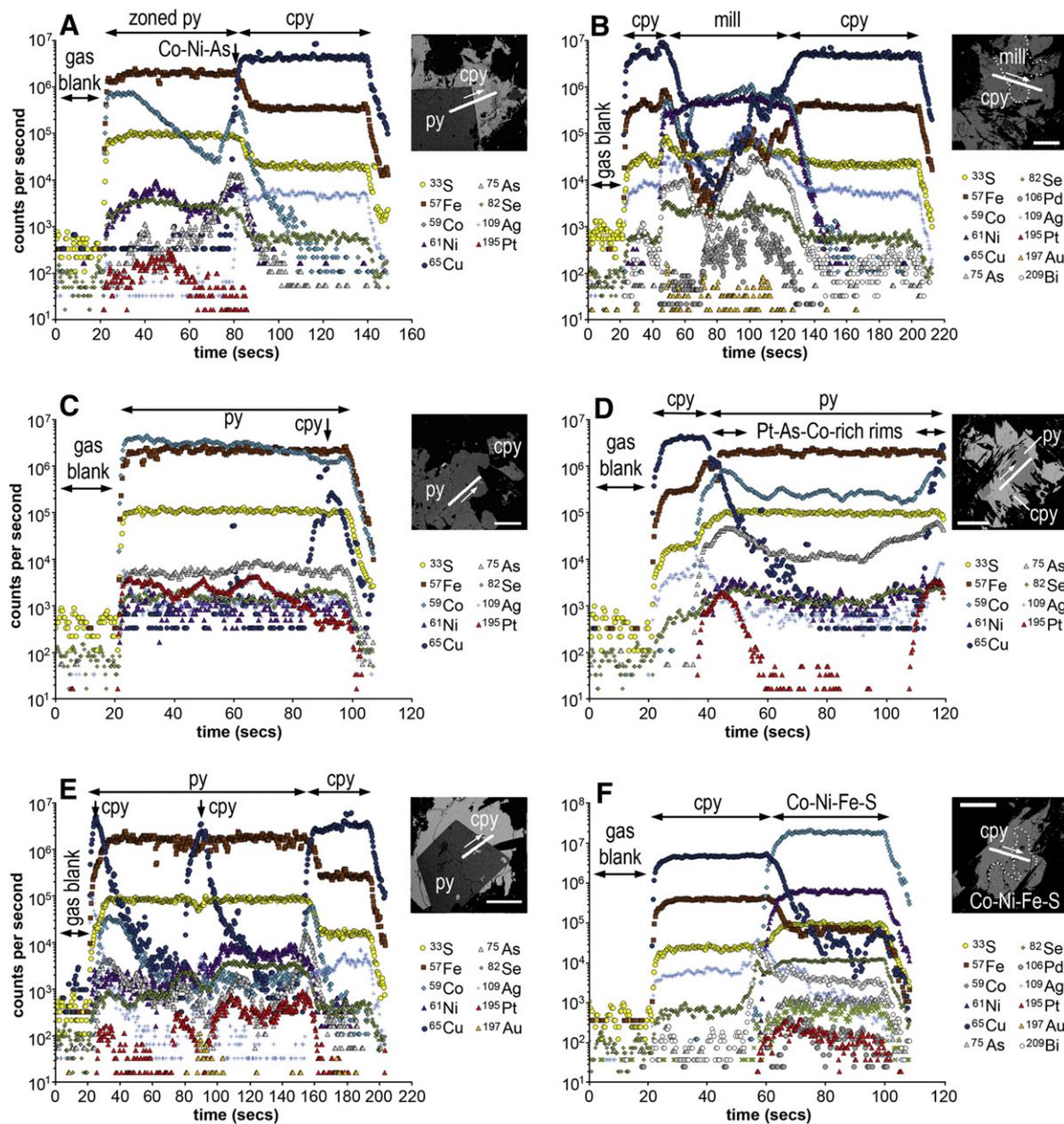
Fig. 13. Time resolved analysis spectra of LA-ICP-MS analyses of sulfides from the Sron Garbh appinite. Each analysis represents a line across the sample as shown by the thick white lines in the inset images. A: euhedral zoned pyrite and chalcopyrite; B: chalcopyrite-millerite-chalcopyrite; C: blebby pyrite with chalcopyrite inclusion; D: disseminated chalcopyrite and euhedral pyrite with zoned rims; E: disseminated euhedral pyrite with chalcopyrite inclusions and chalcopyrite; F: chalcopyrite and Co-Ni-Fe sulfide. Abbreviations: py: pyrite; cpy: chalcopyrite; mill: millerite.

mineralogy may record alteration and recrystallization of the PGM, they are invariably linked with sulfide minerals, and we propose crystallisation of Te- Bi- and As-PGM from the fractionation of a primary Cu-PGE-Te-Bi-Au-rich sulfide liquid (Helmy et al., 2007; Tomkins, 2010; Holwell and McDonald, 2010).

A key finding of our work has shown that the observed PGM assemblages, which are overwhelmingly dominated by Pd minerals, are not consistent with the bulk rock Pt/Pd ratios, which indicate that there is more Pt in the rock than is represented by the Pt-bearing PGM. The close correlation in bulk rock between Pt, and Pd, Cu and Ni shows that Pt is associated with sulfides and major decoupling of Pt, for example by hydrothermal activity, is unlikely. The LA work on the sulfides provides an explanation of this with Pt proven to be present in pyrite (both textural types) and in Co-Ni-Fe sulfides in concentrations of up

to a few ppm in solid solution. The relative abundance of pyrite versus Co-Ni-Fe sulfides is very high, and thus pyrite is the dominant host for Pt as a trace element in sulfide.

The presence of PGE in solid solution in magmatic sulfides is well documented, although in most cases, Pd, Rh and the IPGE are the most common elements to be found in sulfides, particularly pyrrhotite (IPGE) and pentlandite (Rh and Pd), whereas Pt is rarely found in sulfides and is present more commonly as PGM (e.g. Cabri et al., 1984; Czamanske et al., 1992; Ballhaus and Ryan, 1995; Ballhaus and Sylvester, 2000; Godel et al., 2007). However, a number of recent studies have shown that pyrite can be a particularly significant host to Pt (and other PGE) in solid solution, commonly in low-temperature assemblages where pyrite ± millerite replaces primary pyrrhotite and pentlandite. Examples include the Great Dyke, Zimbabwe (<233 ppm

Table 6
Sulfur isotope data for sulfides hosted within the Sron Garbh appinite (app) and diorite (dio), and the MGP (psam).

Drill hole	Sample number	Rock type	Style	Sulfide	$\delta^{34}S$ (‰ VCDT)
35	10.8	App	Blebby pyrite	Pyrite	+ 1.0
N/A	32312 33120	App	Disseminated pyrite-chalcopyrite	Pyrite	+ 1.1
N/A	32312 33120	App	Disseminated pyrite-chalcopyrite	Pyrite	+ 1.4
N/A	323401 33202	App	Disseminated pyrite-chalcopyrite	Pyrite	+ 2.8
N/A	32406 33133 (3)	App	Disseminated pyrite-chalcopyrite	Pyrite	+ 3.1
N/A	323401 33202	App	Disseminated pyrite-chalcopyrite	Pyrite	+ 3.2
N/A	32406 33133 (1)	App	Disseminated pyrite-chalcopyrite	Chalcopyrite	+ 3.3
33	10.6	App	Disseminated pyrite-chalcopyrite	Pyrite	+ 3.4
35	9.1	App	Disseminated pyrite-chalcopyrite	Pyrite	+ 3.5
37	14.63	App	Disseminated pyrite-chalcopyrite	Pyrite	+ 3.5
35	12.22	App	Blebby pyrite	Pyrite	+ 3.6
N/A	32422 33035	Dio	Disseminated pyrite	Pyrite	+ 3.9
N/A	32406 33133 (2)	App	Blebby pyrite	Pyrite	+ 4.2
33	1.06	Dio	Disseminated pyrite	Pyrite	+ 4.3
35	14.17	Dio	Disseminated pyrite	Pyrite	+ 4.3
36	25.31	Dio	Disseminated pyrite	Pyrite	+ 4.8
35	15.88	Psam	Metasedimentary pyrite	Pyrite	+ 4.9
35	17.04	Psam	Metasedimentary pyrite	Pyrite	+ 5.3

Pt, Oberthür et al., 1997), Aguablanca, Spain (<15 ppm Pt, Piña et al., 2012), the Lac des Iles Complex, Canada (~1 ppm Pt, Djon and Barnes, 2012) and the GNPA member of the northern Bushveld Complex, South Africa (<63 ppm Pt, Smith et al., 2014). Primary pyrite that has crystallised directly from monosulfide solid solution (mss) has also been shown to host Pt (the Great Dyke, <99 ppm Pt, Piña et al., 2016). Our results of several ppm Pt in pyrite (Table 5) in both primary and secondary pyrite are comparable with these other deposits and whatever the mechanism of enrichment, pyrite is the major host for Pt in Sron Garbh.

Barkov et al. (1997) were the first to recognise significant Pt hosted by pyrite and highlighted how Pt^{2+} and Fe^{2+} have a similar ionic radius and therefore Pt could be substituted into FeS_2. Pyrite and sperrylite ($PtAs_2$) have a similar crystal structure and the Fe^{2+} site in pyrite is a suitable place for Pt^{2+} to occupy (Barkov et al., 1997; Piña et al., 2012). Piña et al. (2012) and Djon and Barnes (2012) outline how the association of Pt with high Co and As bearing pyrite suggest As and Co aid the process by distorting the pyrite crystal lattice. Cobalt-nickel rich pyrite is also believed to be a major repository of PGE associated with late stage hydrothermal processes in epithermal systems (Hanley et al., 2010), and the association of Pt with Co and Ni is also shown in its presence in hengleinite at Sron Garbh. Piña et al. (2012) and Djon and Barnes (2012) also suggest hydrothermal fluids may dissolve and redistribute Pt and As into secondary forming pyrite. Although the PGE mineralisation at Sron Garbh is genetically magmatic in origin, this could provide an explanation for the presence of Pt and As in the secondary, blebby pyrite.

10.5. Cu, PGE and Au enrichment in lamprophyric magmas

The presence of elevated Cu, Ni, PGE and Au (with associated semi metals) in magmatic sulfides are more indicative of mafic-ultramafic magmas from a primary mantle origin, rather than calc-alkaline magmas derived from the melting of a metasomatised mantle wedge. The Mordor Alkaline Igneous Complex is an example of Cu-Ni-PGE mineralisation hosted in a cumulate layer from a lamprophyric magma (Barnes et al., 2008) and thus is the closest analogy to Sron Garbh outside of Scotland. Both Sron Garbh and Mordor are strongly PPGE enriched over the IPGE, with high Pd/Ir ratios (Fig. 12). Both are relatively enriched in Au as well, with a distinct peak at Au in most of the primitive mantle normalised profiles in Fig. 12. Sron Garbh is more enriched in Cu and Ni, but both are relatively Cu-rich compared to Ni. As such, both intrusions can be classed as having Cu-Ni-Pt-Pd-Au magmatic sulfide mineralisation.

As discussed above, the Cu-rich nature of the sulfide could be due to the stage of fractionation at which the magma attained sulfide saturation. The later this happens, the more Cu-, Au- and PPGE-enriched the resultant sulfide will be as the IPGE and Ni are more compatible during silicate liquid fractionation and thus this could easily explain the relatively low Ni, and very low IPGE contents. The prominent Ru anomaly seen in our data and that of the Mordor rocks (Fig. 12), is likely due to chromite fractionation prior to emplacement, with such anomalies commonly observed on whole rock PGE profiles of moderately evolved volcanic rocks (Arguin et al., 2016). This again would imply fractionation of the magma before sulfide saturation.

However, there are other possible reasons that are related to the source regions for the lamprophyric melts. Lorand et al. (2013) indicate that 'refertilisation' processes in the upper mantle can produce significantly PPGE, Au, Cu and Se enriched zones through mantle metasomatism, which can precipitate BMS enriched in these elements. Lorand et al. (2013) also state that major magmatic inputs at the lithosphere-asthenosphere boundary can 'refertilise' old PGE-rich harzburgitic protoliths with new PPGE-rich BMS. These processes can be on a regional scale (100 km) and represent PPGE-Au-Cu-Se-fertile upper lithospheric mantle. The source of magma for the post-collisional magmatism in Scotland, including Sron Garbh and other lamprophyric intrusions is proposed to be through hydrous melting of a metasomatised mantle wedge (Fowler and Henney, 1996; Fowler et al., 2001). If this had undergone significant refertilisation in the way described by Lorand et al. (2013), then this may be a reason for the relatively high number of PGE sulfide occurrences in lamprophyric magmas in the region, and critically, and explanation of the characteristic base and precious metal characteristics.

Alternatively, the apparent fractionation of PPGE over IPGE may more likely be linked with the degree of partial melting of the source. According to conventional mantle melting models, residual sulfide will remain in the mantle, sequestering PGEs (Keays, 1995; Crocket, 2002; Crocket and Paul, 2004). However, Sisson (2003) and Mungall et al. (2006) suggest high oxidation states and the presence of sulphate rather than sulfide allows the liberation of PGEs contained within the sulfide to produce PGE enriched magma. Furthermore, and most intriguingly, the model of incongruent melting, or partial melting of mantle sulfides, whereby the PPGE are liberated into early melting products (e.g. Ballhaus et al., 2006), and the IPGE are left behind in mss could explain the PPGE enrichment in some mantle melts.

A variant on the incongruent melting model would be if pre-existing PGE-BMS assemblages are present in the source region. Typical
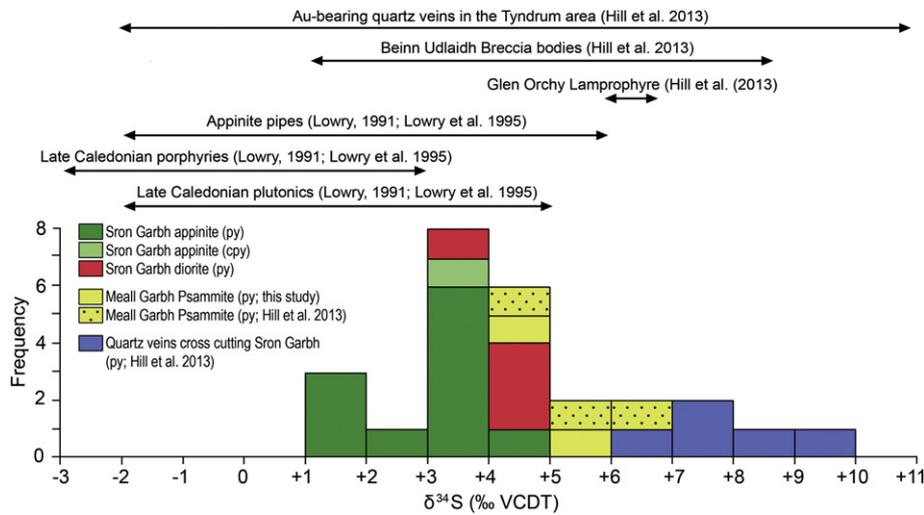
Fig. 14. Sulfur isotope data for sulfides from Sron Garbh and associated country rocks. Ranges are also shown for regional intrusions and vein mineralisation from Lowry (1991), Lowry et al. (1995) and Hill et al. (2013).

assemblages would contain pyrrhotite-pentlandite-chalcopyrite (mss-iss) with associated PGM such as Pt and Pd tellurides, plus Au minerals. In a reverse of the well-established fractionation of sulfide-semi metal liquids on cooling (e.g. Holwell and McDonald, 2010), the first phases to melt, at temperatures lower than 900 °C, would be the Pt and Pd-semimetal and Au-bearing minerals, followed by the Cu-rich sulfide, with IPGE potentially held back in the Fe-Ni sulfide portion, which has the highest solidus temperature. As such, this could produce low-degree partial melts that are Cu-, PPGE-, Au- and semi metal-enriched. The slab drop off event could provide the essential heat source to remelt lower crustal or lithospheric mantle material in this way. A further condition of this would be that magmatic sulfide accumulations were present in the source region, which may not necessarily be common, but this may explain the relative rarity of mineralised appinites. We suggest that incongruent melting of pre-existing Ni-Cu-PGE-semi metal sulfides or 'refertilised' mantle can produce lamprophyric magmas that, should they become sulfide saturated, will produce characteristically Cu-PPGE-Au-semi metal ores.
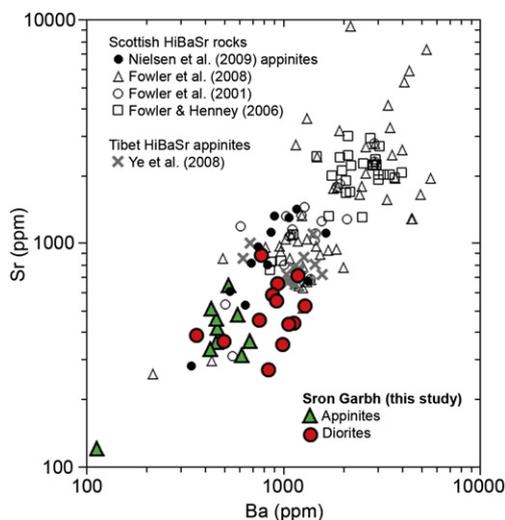
10.6. A model for the emplacement of Sron Garbh and Cu-Ni-PGE-Au sulfide generation

Fig. 16 illustrates a schematic model for the development of the petrogenesis, emplacement and mineralisation in the Sron Garbh intrusion based on the data presented in this paper. During closure of the Iapetus Ocean, metasomatic enrichment of the mantle wedge provided the geochemically distinctive protolith for the HiBaSr lamprophyric magmas. Following the ocean closure and the post-collisional slab drop off (Fig. 16A), low degree partial melting of a hydrated and metasomatised mantle wedge produced a lamprophyric melt (Neilson et al., 2009). In addition, a key factor in generating a Cu-PPGE-Au enriched melt is that the slab drop-off event provided the necessary heat to induce low degree partial melting, liberating Cu, PPGE, Au and semi metals into the melt from 'refertilised' mantle or via incongruent melting of pre-existing Ni-Cu-PGE sulfides.

During the ascent, sulfide saturation occurred, most likely by assimilation of crustal S from the Dalradian sediments and stratabound mineralised horizons, producing a sulfide liquid that was enriched in Cu, PPGE and Au as it ascended through the magmatic plumbing system of Sron Garbh (Fig. 16B). The Sron Garbh intrusion was emplaced through various magma pulses; first creating the amphibole cumulate layers with disseminated magmatic sulfides (Fig. 6B), then the dioritic portion (Fig. 6C). The presence of PGE-rich disseminated chalcopyrite-pyrite mineralisation and the lower grade blebby pyrite-dominant mineralisation may be the original product of multiple pulses. The most PGE-rich sulfide is present in the most amphibole-rich appinite, and may represent the earliest, most mafic end member. Although field relationships are ambiguous, we interpret the current outcrop pattern as evidence that Sron Garbh represents the basal section of a sill, rather than two distinct pipe-like intrusions (Fig. 4A). The unusual magmatic sulfide assemblage of chalcopyrite and Pt-bearing pyrite with minor Ni-Co-As sulfides and Pd-Te-Bi PGM formed on cooling and was later recrystallized with the addition of low temperature, Co, As-rich pyrite and minor Pd antimonides with no significant base and precious metal mobilisation (Fig. 6C).

10.7. Implications for the prospectivity of alkaline magmatic systems

The general processes involved in the generation of magmatic sulfide deposits, so well established for mafic-ultramafic systems (e.g. Naldrett, 2011), appears to be applicable in low-degree hydrous

Fig. 15. Scatterplot showing Ba and Sr in the Sron Garbh rocks compared to rocks of the HiBaSr suite in Scotland (mostly granites), and comparable HiBaSr appinite-granites in Tibet.
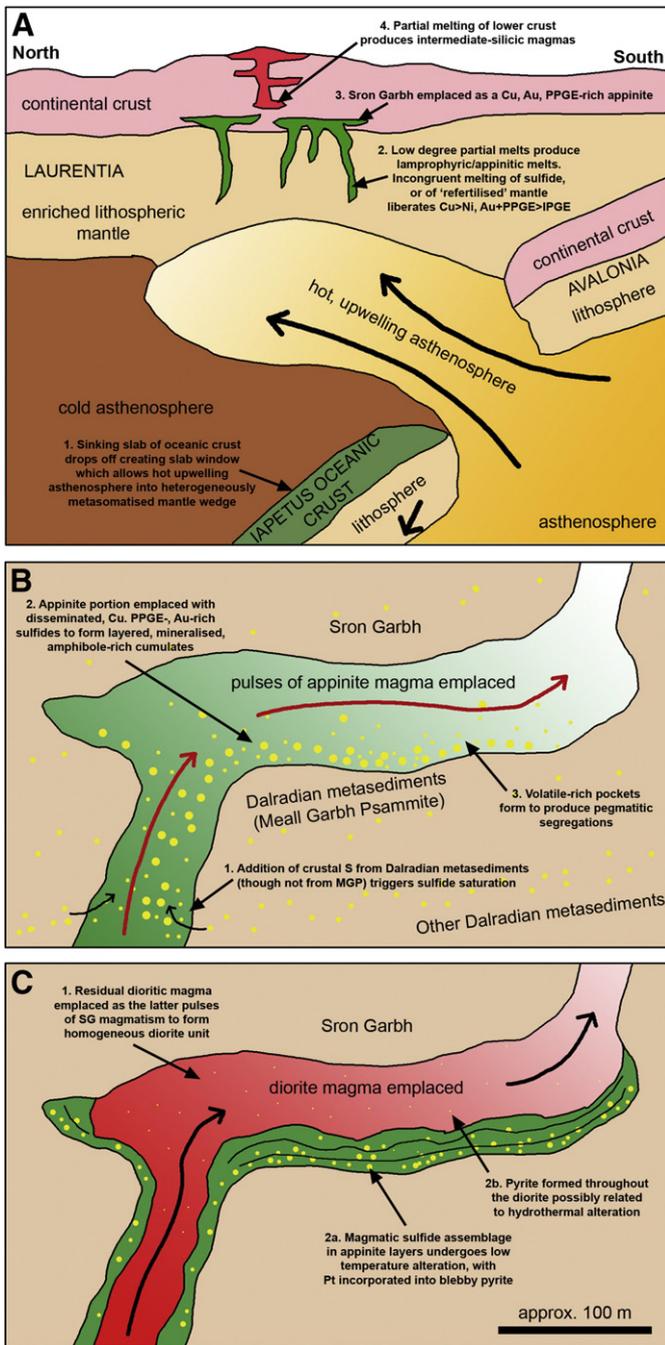
Fig. 16. Schematic model showing the emplacement of Sron Garbh. A: following the closure of the Iapetus Ocean and the continent-content collision of Avalonia and Laurentia, slab drop off allowed upwelling asthenosphere into the mantle wedge, producing low-degree partial melts that are emplaced as appinites (after Nielsen et al. 2009). B: The Sron Garbh intrusion is emplaced first as an appinitic, Cu-PPGE-Au-bearing sulfide magma, with S sourced from Dalradian metasediments at depth; C: the latter pulses of Sron Garbh emplacement form the PGE-poor dioritic portion.

located in the Grampian terrane (Fig. 1) and is unlikely to have been formed in the same setting as Sron Garbh, so there remain questions as to why Scotland contains such occurrences over a wide area with differing geological histories. The answer may lie in the sporadic presence of pre-existing Ni-Cu-PGE sulfides in the source regions. From our observations and interpretations on Sron Garbh at least, constraints that need to be met in order to produce a similar PGE bearing suite include the melting of metasomatised mantle, which is suitably enabled by a slab drop off event in a post-collisional tectonic setting. Low degree and low temperature partial melts permit fractionation of the PPGE, Au and semi metals from the IPGE, and Cu from Ni, as do 'refertilisation' processes in the mantle sources. Melts sourced in this way can then produce characteristically Cu-PPGE-Au-semi metal enriched mineralisation. Attaining sulfide saturation is a pre-requisite for magmatic sulfide ore formation and the chances of this occurring are increased with the presence of S-bearing country rocks. In the Scottish case, the folded Dalradian metasediments have a number of syn-sedimentary sulfide-bearing horizons located at depth that may also have contributed to mineralisation. The voluminous post-collisional granites located through the Caledonides are commonly spatially and temporally associated with appinite intrusions. However, appinites are often misclassified and therefore the variability, distribution and PGE potential of the appinite intrusions are potentially unrealised and underexplored.

11. Conclusions

Sron Garbh represents an unconventional Cu-Ni-PGE-Au prospect hosted by appinitic cumulates. The style of mineralisation at Sron Garbh is characteristically chalcopyrite-pyrite dominant, with Pt in solid solution in pyrite, and Pd as primary and secondary PGM. This example adds to several recent studies that have identified pyrite as an important repository of Pt. The identification of PGE mineralisation in Sron Garbh and other similar suites located in Scotland and elsewhere in the world imply they do have some potential to contain economic concentrations of PGEs. However, given their relatively rare occurrence, a specific set of pre-requisite factors may have been involved in the development of mineralisation, including: the degree of mantle melting and remelting, the presence of pre-existing Ni-Cu-PGE sulfides in the source regions, the post-collision tectonic setting, and the ability to interact with S-bearing country rocks. The tectonic setting of the Scottish occurrences is consistent with slab drop off processes that allow hydrous remelting of the mantle wedge which can then become the source of the Cu-Au-PPGE-enriched alkaline melts.

melts as well. Prospects such as Sron Garbh and the Mordor Alkaline Igneous Complex demonstrate that lamprophyric magmas may be important carriers of PGE although their scarcity implies that specific conditions are likely to be necessary to produce mineralisation. However, the presence of PGE-enriched sulfides in lamprophyric intrusions appears to be relatively common across the Scottish Caledonides (Power et al., 2004; Styles et al., 2004), indicating that the region contains certain features that make it more prospective than other alkaline provinces worldwide. That said, Talnotry is not

Appendix A

Table A1
Full geochemistry for SGAQ14 (Scotgold assays)

Sample no.	Rock type	Auppb	Pdppb	Ptppb	Ag	Al	As	Ba	Be	Bi	Ca	Cd	Ce	Co	Cr	Cu	Fe	Ga	Ge	Hg	K	La	Li
					ppm	%	ppm	ppm	ppm	ppm	%	ppm	ppm	ppm	ppm	ppm	%	ppm	ppm	ppm	%	ppm	ppm
SAGQ14-01	SGD	<2	20	18	<0.5	5.14	1.4	118	1	0.07	7.41	0.19	38.3	32.3	1214	65.6	4.43	11.8	1.4	<0.01	0.29	20.5	6
SAGQ14-02	SGD	2	42	34	<0.5	6.20	5.3	517	<1	0.11	6.41	0.16	29.7	45.7	578	184.1	7.65	14.6	1.7	0.02	1.34	14.5	10
SAGQ14-03	SGD	<2	<2	<2	<0.5	7.59	4.1	616	1	<0.05	4.80	0.10	34.6	32.8	168	136.9	7.64	17.8	1.3	0.01	2.25	16.6	14
SAGQ14-04	SGD	3	<2	<2	<0.5	8.14	3.9	654	1	0.08	5.41	0.11	36.0	32.4	113	157.4	8.30	19.4	1.2	0.01	2.34	17.0	18
SAGQ14-05	SGD	4	<2	<2	<0.5	7.65	3.1	576	1	0.07	6.02	0.19	32.8	37.6	89	201.7	9.83	18.7	1.2	<0.01	2.28	14.6	16
SAGQ14-06	SGD	9	<2	<2	<0.5	7.82	4.2	637	1	0.10	5.50	0.19	37.8	33.7	103	180.1	8.14	19.1	1.2	0.02	2.18	18.1	23
SAGQ14-07	SGD	<2	<2	<2	<0.5	8.10	4.8	705	2	<0.05	4.79	0.12	39.2	25.7	121	75.8	7.23	19.1	1.1	0.01	2.56	18.8	23
SAGQ14-08	SGD	<2	<2	2	<0.5	8.24	5.9	697	1	0.08	4.42	0.10	42.9	25.3	154	53.7	6.94	18.7	1.1	0.05	2.80	22.7	22
SAGQ14-09	SGD	<2	<2	<2	<0.5	8.46	5.9	782	1	<0.05	4.66	0.12	39.9	24.3	143	51.2	6.62	18.9	1.1	0.01	3.00	21.3	20
SAGQ14-10	SGD	<2	<2	<2	<0.5	8.44	5.4	839	1	0.08	5.06	0.13	33.3	30.3	107	96.8	6.83	18.9	1.0	0.02	3.01	16.9	16
SAGQ14-11	App	6	36	29	<0.5	4.65	29.0	459	1	0.07	7.94	0.09	20.1	47.1	893	299.9	6.16	10.9	1.4	<0.01	1.15	10.0	16
SAGQ14-12	App	6	74	56	<0.5	3.17	11.4	287	<1	0.09	11.72	0.46	16.2	46.0	881	711.0	5.23	7.9	1.5	0.03	0.69	7.7	11
SAGQ14-13	App	185	563	410	3.9	3.55	51.1	268	<1	0.30	7.01	2.42	16.9	276.1	885	6115.1	10.75	8.9	1.6	<0.01	0.68	8.1	7
SAGQ14-14	App	2	32	26	<0.5	2.87	1.9	275	<1	0.12	11.13	0.14	15.3	42.5	867	156.1	4.63	6.7	1.6	0.02	0.43	7.8	7
SAGQ14-15	App	4	21	22	<0.5	4.78	2.8	509	<1	<0.05	9.27	0.12	21.9	29.9	598	129.7	5.54	11.2	1.5	0.03	1.17	10.8	18
SAGQ14-16	App	3	<2	<2	<0.5	7.16	4.0	569	1	0.08	5.02	0.07	30.4	33.7	89	138.9	8.32	17.5	1.5	0.01	2.48	14.5	26

Table A1 (*continued*)

Sample no.	Mg	Mn	Mo	Na	Nb	Ni	P	Pb	Rb	Re	S	Sb	Sc	Se	Sn	Sr	Ta	Te	Th	Ti	Tl	U	V	W	Y	Zn	Zr
	%	ppm	ppm	%	ppm	ppm	%	ppm	ppm	ppm	%	ppm	ppm	ppm	ppm	ppm	ppm	ppm	ppm	ppm	ppm	ppm	ppm	ppm	ppm	ppm	ppm
SAGQ14-01	6.63	1255	0.38	2.07	4.64	155.4	0.046	14.8	7.5	<0.2	0.10	0.16	38.5	<0.5	0.9	358	0.31	0.30	3.9	2397	0.06	1.2	121	60.1	15.8	81.5	112
SAGQ14-02	6.59	1222	0.25	1.54	4.40	94.6	0.102	6.8	43.4	<0.2	0.65	0.27	44.5	<0.5	1.4	420	0.30	0.24	2.4	7059	0.28	0.8	317	16.6	18.8	90.5	81
SAGQ14-03	4.31	1066	0.39	1.87	5.83	13.1	0.136	8.7	79.4	<0.2	0.66	0.27	30.7	<0.5	1.5	703	0.42	0.35	3.1	7871	0.51	1.0	345	1.0	21.5	95.4	94
SAGQ14-04	3.98	1179	0.14	1.68	5.60	9.0	0.238	11.1	85.1	<0.2	0.77	0.26	27.7	<0.5	3.7	748	0.35	0.30	2.7	7754	0.53	1.0	349	3.5	22.1	109.5	86
SAGQ14-05	4.64	1250	0.25	1.43	4.93	11.0	0.349	13.6	74.0	<0.2	0.83	0.19	30.3	<0.5	1.7	689	0.32	0.31	2.0	8520	0.47	0.8	419	1.0	22.8	120.8	71
SAGQ14-06	3.97	1075	0.13	1.72	4.72	10.4	0.249	13.7	69.7	<0.2	0.87	0.19	26.6	<0.5	1.4	688	0.33	0.42	2.8	5725	0.40	1.0	332	1.6	19.7	101.8	80
SAGQ14-07	3.25	1102	0.30	1.79	5.88	10.5	0.250	21.7	84.8	<0.2	0.45	0.24	20.5	<0.5	1.4	771	0.44	0.33	3.6	5439	0.53	1.1	292	1.8	20.5	107.0	105
SAGQ14-08	3.19	1058	0.11	1.94	6.37	10.2	0.231	21.5	100.4	<0.2	0.39	0.26	20.5	<0.5	1.4	743	0.44	0.41	4.3	5967	0.67	1.3	275	0.6	20.9	99.7	117
SAGQ14-09	2.97	1005	0.32	1.79	5.77	9.7	0.259	31.6	113.2	<0.2	0.41	0.30	18.6	<0.5	1.3	692	0.40	0.27	3.8	5549	0.72	1.2	262	1.1	18.7	102.2	100
SAGQ14-10	3.21	927	0.12	1.64	4.83	13.0	0.198	26.8	122.8	<0.2	0.67	0.41	22.0	<0.5	1.2	644	0.35	0.38	3.4	5640	0.80	1.2	276	0.9	17.2	92.8	94
SAGQ14-11	7.15	1222	0.23	0.58	2.27	197.2	0.073	8.3	49.2	<0.2	0.43	0.79	41.8	<0.5	0.7	293	0.13	0.23	1.7	3501	0.34	0.6	201	1.5	12.0	81.7	49
SAGQ14-12	7.56	1470	0.07	0.43	2.06	342.1	0.035	11.6	24.6	<0.2	0.32	0.41	34.6	<0.5	0.7	426	0.15	0.28	1.2	3000	0.17	0.4	153	<0.1	11.5	66.5	43
SAGQ14-13	7.43	1096	0.64	0.50	2.77	1602.0	0.044	7.4	20.4	<0.2	5.82	0.43	31.8	9.3	1.0	310	0.19	0.29	1.4	3150	0.15	0.5	144	<0.1	10.6	89.3	48
SAGQ14-14	8.12	1432	0.09	0.41	1.98	283.0	0.031	9.9	11.7	<0.2	0.10	0.47	35.1	<0.5	0.5	521	0.12	0.21	1.2	2536	0.08	0.4	124	<0.1	9.4	59.1	40
SAGQ14-15	5.06	1190	0.28	0.94	3.35	68.9	0.134	9.9	52.3	<0.2	0.68	0.54	26.2	0.5	1.0	799	0.21	0.32	2.0	4033	0.38	0.8	181	0.4	12.9	67.6	56
SAGQ14-16	4.14	1079	0.08	1.28	4.44	9.5	0.197	9.4	113.1	<0.2	0.99	0.62	27.1	<0.5	1.7	442	0.26	0.31	2.7	6925	0.80	1.0	335	0.9	19.5	105.3	78

References

Andersen, J.C.Ø., Power, M.R., Pirrie, D., Shail, R.K., Rollinson, G.K., 2010. Platinum-group minerals in the Craignure Cu-Ni-sulfide deposit, Scotland. 11th International Platinum Symposium.

Anderton, R, 1985. Sedimentation and tectonics in the Scottish Dalradian. Scott. J. Geol. 21, 407–436.

Arguin, J.-P., Pagé, P., Barnes, S.-J., Yu, S.-Y., Song, X.-Y., 2016. The effect of chromite crystallization on the distribution of osmium, iridium, ruthenium and rhodium in picritic magmas: an example from the Emeishan Large Igneous Province, Southwestern China. J. Petrol. 57, 1019–1048.

Arndt, N.T., 2011. Norilsk-Talnakh Region, Siberia: insights into geological setting & origin of Ni-Cu-PGE sulfide deposits. Rev. Econ. Geol. 17, 199–215.

Atherton, M.P., Ghani, A.A., 2002. Slab breakoff: a model for Caledonian, Late granite syn-collisional magmatism in the orthotectonic (metamorphic) zone of Scotland and Donegal, Ireland. Lithos 62, 65–85.

Ballhaus, C., Ryan, C.G., 1995. Platinum-group elements in the Merensky reef. I. PGE in solid solution in base metals sulfides and the down-temperature equilibration history of Merensky ores. Contrib. Mineral. Petrol. 122, 241–251.

Ballhaus, C., Sylvester, P., 2000. PGE enrichment processes in the Merensky reef. J. Petrol. 41, 454–561.

Ballhaus, C., Bockrath, C., Wohlgemuth-Ueberwasser, C., Laurenz, V., Berndt, J., 2006. Fractionation of the noble metals by physical processes. Contrib. Mineral. Petrol. 152, 667–684.

Barkov, A.Y., Halkoaho, T.A.A., Kaajoki, K.V.O., Alapieti, T.T., Peura, R.A., 1997. Ruthenian pyrite and nickeloan malarite from the Imandra layered complex, northwestern Russia. Can. Mineral. 35, 887–897.

Barnes, S.J., 2006. Komatiite-hosted nickel sulfide deposits: geology, geochemistry, and genesis. Society of Economic Geologists Special Publication, 13, pp. 51–118.

Barnes, R.P., Rock, N.M.S., Gaskarth, J.W., 1986. Late Caledonian dyke-swarms in Southern Scotland: new field, petrological and geochemical data for the Wigtown Peninsula, Galloway. Geol. J. 21, 101–125.

Barnes, S.J., Anderson, J.A.C., Smith, T.R., Bagas, L., 2008. The Mordor Alkaline Igneous Complex, Central Australia: PGE-enriched disseminated sulfide layers in cumulates from a lamprophyric magma. Mineral. Deposita 43, 641–662.

Barnes, S.J., Cruden, A.R., Arndt, N., Saumur, B.M., 2016. The mineral system approach applied to magmatic Ni–Cu–PGE sulphide deposits. Ore Geol. Rev. 76, 296–316.

Cabri, L.J., Blanks, H., El Gorsey, A., Laflamme, J.H.G., Nobiling, R., Sizgoric, M.B., Traxel, K., 1984. Quantitative trace-element analyses of sulphides from Sudbury and Stillwater by proton microprobe. Can. Mineral. 22, 521–542.

Campbell, I.H., Naldrett, A.J., Barnes, S.J., 1983. A model for the origin of platinum-rich sulphide horizons, in the Bushveld and Stillwater Complexes. J. Petrol. 24, 133–165.

Conliffe, J., Selby, D., Porter, S.J., Feely, M., 2010. Re-Os molybdenite dates from the Ballachulish and Kilmelford Igneous complexes (Scottish Highlands): age constraints for late Caledonian magmatism. J. Geol. Soc. Lond. 167, 297–302.

Cowie, J.W., Rushton, A.W.A., Stubblefield, C.J., 1972. A correlation of the Cambrian rocks in the British Isles. Geological Society, London, Special Reports vol. 2.

Craig, J.R., 1973. Pyrite-pentlandite and other low temperature relations in the Fe-Ni-S system. Am. J. Sci. 2734, 496–510.

Crocket, J.H., 2002. Platinum-group elements in basalts from Maui, Hawaii: low abundances in alkali basalts. Can. Mineral. 40, 595–609.

Crocket, J.H., Paul, D.K., 2004. Platinum-group elements in Deccan mafic rocks: a comparison of suites differentiated by Ir content. Chem. Geol. 208, 273–291.

Curtis, S.F., Pattrick, R.A.D., Jenkin, G.R.T., Fallick, A.E., Boyce, A.J., Treagus, J.E., 1993. Fluid inclusion and stable isotope study of fault-related mineralization in Tyndrum area, Scotland. Applied Earth Science (Transaction of the Institute of Mining and Metallurgy B) 102, B39–B47.

Czamanske, G.K., Kunilove, V.R., Zientek, M.L., Cabri, L.J., Likhachev, A.P., Calk, L.C., Oscarson, R.L., 1992. A proton-microprobe study of sulfide ores from the Norilsk-Talnakh district Siberia. Can. Mineral. 30, 249–287.

Dalradian Resources Inc, 2012. A Preliminary Economic Assessment of the Curraghinalt Gold Deposit, Tyrone Project, Northern Ireland. Micon International Limited, Toronto.

Dare, S.A.S., Barnes, S.-J., Prichard, H.M., Fisher, P.C., 2011. Chalcophile and platinum-group element (PGE) concentrations in the sulfide minerals from the McCreedy East deposit, Sudbury, Canada, and the origin of PGE in pyrite. Mineral. Deposita 46, 381–407.

Djon, M.L.N., Barnes, S.-J., 2012. Changes in sulfides and platinum-group minerals with the degree of alteration in the Roby, Twilight and High grade zones of the Lac des Iles Complex, Ontario, Canada. Mineral. Deposita 47, 875–896.

Eckstrand, O.R., Hulbert, L.J., 1987. Selenium and the source of sulfur in magmatic nickel and platinum deposits (abs). Geological Association of Canada–Mineralogical Association Canada Program with Abstracts. v.12, p. 40.

Fowler, M.B., Henney, P.J., 1996. Mixed Caledonian appinite magmas: implications for lamprophyre fractionation and high Ba-Sr granite genesis. Contrib. Mineral. Petrol. 126, 199–215.

Fowler, M.B., Henney, P.J., Darbyshire, D.P.F., Greenwood, P.B., 2001. Petrogenesis of high Ba-Sr granites: the Rogart pluton, Sutherland. J. Geol. Soc. Lond. 158, 521–534.

Fowler, M.B., Kocks, H., Darbyshire, D.P.F., Greenwood, P.B., 2008. Petrogenesis of high Ba-Sr plutons from the Northern Highlands Terrane of the British Caledonian Province. Lithos 105, 129–148.

Galantas Gold Corporation, 2013. Technical Report on the Omagh Gold Project, County Tyrone, Northern Ireland. AIM Announcement, 23rd July 2013.

Godel, B., Barnes, S.-J., Maier, W.D., 2007. Platinum-group elements in sulphide minerals, platinum-group minerals, and whole-rocks of the Merensky Reef (Bushveld Complex, South Africa): implications for the formation of the reef. J. Petrol. 48, 1569–1604.

Gunn, A.G., Styles, M.T., 2002. Platinum-group element occurrences in Britain: magmatic, hydrothermal and supergene. Applied Earth Science (Trans. Instn Min. Metall. Section B) 111, B2–B14.

Halliday, A.N., Stephens, W.E., 1984. Crustal controls on the genesis of 400 Ma old Caledonian granites. Phys. Earth Planet. Inter. 35, 89–104.

Hamidullah, S., 2007. Petrography and mineral chemistry as indicators of variations of crystallization conditions in the Loch Lomond and appinite suites, western Scotland. Proceedings of the Geologists' Association Journal 118, 101–115.

Hanley, J.J., MacKenzie, M.K., Warren, M.R., Guillong, M., 2010. Distribution and origin of platinum-group elements in Alkalic porphyry Cu-Au and low sulfidation epithermal Au deposits in the Canadian Cordillera. 11th Platinum Symposium.

Helmy, M.H., Ballhaus, C., Berndt, J., Bockrath, C., Wohlgemuth-Ueberwasser, C., 2007. Formation of Pt, Pd and Ni tellurides: experiments in sulfide-telluride systems. Contrib. Mineral. Petrol. 153, 577–591.

Rice, C.M., 2013. How the Neoproterozoic S-isotope record illuminates the genesis of vein gold systems: an example from the Dalradian Supergroup in Scotland 2015 In: Hill, N.J., Jenkin, G.R.T., Boyce, A.J., Sangster, C.J.S., Catterall, D.J., Holwell, D.A., Naden, J., Jenkin, G.R.T., Lusty, P.A.J., McDonald, I., Smith, M.P., Boyce, A.J., Wilkinson, J.J. (Eds.), Ore Deposits in an Evolving Earth. Geological Society, London, Special Publications vol. 393, pp. 213–247.

Holwell, D.A., McDonald, I., 2010. A review of the behaviour of platinum group elements within natural magmatic sulfide ore systems. Platin. Met. Rev. 54, 26–36.

Holwell, D.A., McDonald, I., Armitage, P.E.B., 2006. Platinum-group mineral assemblages in the Platreef at the Sandsloot Mine, northern Bushveld Complex, South Africa. Mineral. Mag. 70, 83–101.

Holwell, D.A., Keays, R.R., Firth, E.A., Findlay, J., 2014. Geochemistry, and mineralogy of platinum-group element mineralization in the River Valley Intrusion, Ontario, Canada: a model for early stage S saturation and multi-stage emplacement and the implications for "contact-type" Ni-Cu-PGE mineralization. Econ. Geol. 109, 689–712.

Hughes, H.S.R., McDonald, I., Boyce, A.J., Holwell, D.A., Kerr, A.C., 2016. Sulphide sinking in magma conduits: evidence from mafic-ultramafic plugs on Rum and the wider North Atlantic Igneous Province. J. Petrol. http://dx.doi.org/10.1093/petrology/egw010.

Keays, R.R., 1995. The role of komatiitic and picritic magmatism and S-saturation in the formation of ore deposits. Lithos 34, 1–18.

Keays, R.R., Lightfoot, P.C., 2004. Formation of Ni-Cu-platinum group element sulfide mineralization in the Sudbury impact melt sheet. Mineral. Petrol. 82, 217–258.

Keays, R.R., Lightfoot, P.C., 2010. Crustal sulphur is required to form magmatic Ni-Cu sulfide deposits: evidence from chalcophile element signatures of Siberian and Deccan Trap basalts. Mineral. Deposita 45, 241–257.

Kelley, S.P., Fallick, A.E., 1990. High precision spatially resolved analysis of δ^{34}S in sulfides using a laser extraction technique. Geochim. Cosmochim. Acta 54, 883–888.

Labidi, J., Cartigny, P., Moreira, M., 2013. Non-chondritic sulphur isotope composition of the terrestrial mantle. Nature 501, 208–211.

Lesher, C.M., 1989. Komatiite-associated nickel sulfide deposits. In: Whitney, J.A., Naldrett, A.J. (Eds.), Ore Deposition Associated With Magmas vol. 4. Economic Geology Publishing Company, El Paso, pp. 44–101.

Lesher, C.M., Keays, R.R., 2002. Komatiite-associated Ni-Cu-PGE deposits: geology, mineralogy, geochemistry and genesis. In: Cabri, L.J. (Ed.), The Geology, Geochemistry Mineralogy and Mineral Beneficiation of Platinum Group Elements. Canadian Institute of Mining Metallurgy and Petroleum Special Volume 54, pp. 579–617.

Lesher, C.M., Arndt, N.T., Grover, D.I., 1984. Genesis of komatiite-associated nickel sulphide deposits at Kambalda, Western Australia: a distal volcanic model. In: Buchanan, D.L., Jones, M.J. (Eds.), Sulphide Deposits in Mafic and Ultramafic Rocks. Institution of Mining and Metallurgy, London, pp. 70–80.

Li, C.S., Maier, W.D., de Waal, S.A., 2002. The role of magma mixing in the genesis of PGE mineralization in the Bushveld Complex: thermodynamic calculations and new interpretations - a reply (letter). Econ. Geol. Bull. Soc. Econ. Geol. 97, 667.

Li, C., Ripley, E.M., Merino, E., Maier, W.D., 2004. Replacement of base metal sulphides by actinolite, epidote, calcite and magnetite in the UG2 and Merensky Reef of the Bushveld Complex, South Africa. Econ. Geol. 99, 173–184.

Li, B., Huang, Z., Zhu, C., 2009. Experimental study on liquid immiscibility of lamprophyre-sulfide melt at high temperature and high pressure and its geological significance. Chin. J. Geochem. 28, 198–203.

Lorand, J.P., Alard, O., Luguet, A., Keays, R.R., 2003. Sulfur and selenium systematics of the subcontinental lithospheric mantle: inferences from the Massif Central xenolith suite (France). Geochim. Cosmochim. Acta 67, 4137–4151.

Lorand, J.P., Luguet, A., Alard, O., 2013. Platinum-group element systematics and petrogenetic processing of the upper mantle: a review. Lithos 164-167, 2–21.

Lowry, D., 1991. The Genesis of Late Caledonian Granitoid-related Mineralisation in Northern Britain (Unpublished PhD thesis) University of St Andrews.

Lowry, D., Boyce, A.B., Fallick, A.E., Stephens, W.E., 1995. Genesis of porphyry and plutonic mineralisation systems in metaluminous granitoids of the Grampian Terrane, Scotland. Trans. Roy. Soc. Edinb. Earth Sci. 85, 221–237.

Maier, W.D., 2005. Platinum-group element (PGE) deposits and occurrences: mineralization styles, genetic concepts, and exploration criteria. Invited presidential review. J. Afr. Earth Sci. 41, 165–191.

McCulloch, M.T., Gamble, J.A., 1991. Geochemical and geodynamical constraints on subduction zone magmatism. Earth Planet. Sci. Lett. 102, 358–374.

McDonald, I., Holwell, D.A., 2011. Geology of the northern Bushveld Complex and the setting and genesis of the Platreef Ni-Cu-PGE deposit. Rev. Econ. Geol. 17, 297–327.

Misra, K.C., Fleet, M.E., 1974. Chemical composition and stability of violarite. Econ. Geol. 59, 391–403.

Moore, P., 2011. Developing an Exploration Guide for the Auriferous Breccia Pipes at Beinn Udlaidh, Scotland (Unpublished MGeol project) University of Leicester.

Mungall, J.E., Hanley, J.J., Arndt, N.T., Debecdelievre, A., 2006. Redox controls on mantle-crust fractionation of platinum-group element: evidence from meimechites and other low degree mantle melts. Proc. Natl. Acad. Sci. U. S. A. 103, 12695–12700.

Naldrett, A.J., 2011. Fundamentals of magmatic sulfide deposits. Rev. Econ. Geol. 17, 1–50.

Naldrett, A.J., Kullerud, G., 1967. A study of the Strathcona mine and its bearing on the origin of the nickel-copper ores of the Sudbury District, Ontario. J. Petrol. 8, 453–531.

Naldrett, A.J., Craig, J.R., Kullerud, G., 1967. The central portion of the Fe-Ni-S system and its bearing on pentlandite exsolution in iron-nickel sulfide ores. Econ. Geol. 62, 826–847.

Naldrett, A., Kinnaird, J., Wilson, A., Yudovskaya, M., Chunnett, G., 2011. Genesis of the PGE-enriched Merensky Reef and chromitite seams of the Bushveld Complex. Rev. Econ. Geol. 17, 235–296.

Neilson, J.C., Kokelaar, B.P., Crowley, Q.G., 2009. Timing, relations and cause of plutonic and volcanic activity of the Siluro-Devonian post-collision magmatic episode in the Grampian Terrane, Scotland. J. Geol. Soc. Lond. 166, 545–561.

Oberthür, T., Cabri, L.J., Weiser, T.W., McMahon, G., Müller, P., 1997. Pt, Pd and other trace element in sulfides of the main sulphide zone, Great Dyke, Zimbabwe: a reconnaissance study. Can. Mineral. 35, 597–609.

Ohmoto, H., Rye, R.O., 1979. Isotopes of sulfur and carbon. In: Barnes, H.L. (Ed.), Geochemistry of Hydrothermal Ore Deposits, 2nd ed Wiley, New York, pp. 509–567.

Oliver, G.J.H., 2001. Reconstruction of the Grampian episode in Scotland: its place in the Caledonian Orogeny. Tectonophysics 332, 23–49.

Oliver, G.J.H., Wilde, S.A., Wan, Y., 2008. Geochronology and geodynamics of Scottish granitoids from the late Neoproterozoic break-up of Rodinia to Palaeozoic collision. J. Geol. Soc. Lond. 165, 661–674.

Pattrick, R.A.D., Boyce, A., MacIntyre, R.M., 1988. Au-Ag vein mineralisation at Tyndrum, Scotland. Mineral. Petrol. 38, 477–485.

Piña, R., Gervilla, F., Barnes, S.-J., Ortega, L., Lunar, R., 2012. Distribution of platinum-group and chalcophile elements in the Aguablanca Ni-Cu sulfide deposit (SW Spain): evidence from a LA-ICP-MS study. Chem. Geol. 302-303, 61–75.

Piña, R., Gervilla, F., Barnes, S.-J., Oberthür, T., Lunar, R., 2016. Platinum-group element concentrations in pyrite from the Main Sulfide Zone of the Great Dyke of Zimbabwe. Mineral. Deposita http://dx.doi.org/10.1007/s00126-016-0642-3.

Plank, T., Langmuir, C., 1998. The chemical composition of subducting sediment and its consequences for the crust and mantle. Chem. Geol. 145, 325–394.

Power, M.R., Pirrie, D., Jedwab, J., Stanley, C.J., 2004. Platinum-group element mineralization in an As-rich magmatic sulphide system, Talnotry, southwest Scotland. The Mineralogical Magazine 62, 395–411.

Prichard, H.M., Knight, R.D., Fisher, P.C., McDonald, I., Zhou, M.-F., Wang, C.Y., 2013. Distribution of platinum-group elements in magmatic and altered ores in the Jinchuan intrusion, China: an example of selenium remobilization by postmagmatic fluids. Mineral. Deposita 48, 767–786.

Ripley, E.M., Li, C., 2003. S isotope exchange and metal enrichment in the formation of magmatic Cu-Ni-(PGE) deposits. Econ. Geol. 98, 635–641.

Ripley, E.M., Li, C., 2011. A review of conduit-related Ni-Cu-(PGE) sulfide mineralization at the Voisey's Bay Deposit, Labrador, and the Eagle Deposit, Northern Michigan. Rev. Econ. Geol. 17, 181–197.

Ripley, E.M., Brophy, J.G., Li, C., 2002. Copper solubility in a basalticmelt and sulfide liquid/silicate melt partition coefficients of Cu and Fe. Geochim. Cosmochim. Acta 66, 2791–2800.

Robinson, B.W., Kusakabe, M., 1975. Quantitative preparation of sulfur dioxide for 34S/32S analyses from sulphides by combustion with cuprous oxide. Anal. Chem. 47, 1179–1181.

Rock, N.M.S., 1984. Nature and origin of calc-alkaline lamprophyres: minettes, vogesites, kersantites and spessartites. Trans. R. Soc. Edinb. Earth Sci. 74, 193–227.

Rogers, G., Dunning, G.R., 1991. Geochronology of appinitic and related granitic magmatism in the W Highlands of Scotland. J. Geol. Soc. Lond. 148, 17–27.

Saunders, A.D., Norry, M.J., Tarney, J., 1988. Origin of MORB and chemically-depleted mantle reservoirs: trace element constraints. J. Petrol. 415–445 Special Lithosphere Issue.

Sisson, T.W., 2003. Native gold in a Hawaiian alkalic magma. Econ. Geol. 98, 643–648.

Smith, J.W., Holwell, D.A., McDonald, I., 2014. Precious and base metal geochemistry and mineralogy of the Grasvally Norite-Pyroxenite-Anorthosite (GNPA) member, northern Bushveld Complex, South Africa; implications for a multistage emplacement. Mineral. Deposita 49, 667–692.

Soper, N.J., Strachan, R.A., Holdsworth, R.E., Gayer, R.A., Greiling, R.O., 1992. Sinistral transpression and the Silurian closure of Iapetus. J. Geol. Soc. Lond. 149, 871–880.

Stephenson, D., Gould, D., 1995. British Regional Geology: The Grampian Highlands. HMSO, London.

Stephenson, D., Mendum, J.R., Fettes, D.J., Leslie, A.G., 2013. The Dalradian rocks of Scotland: an introduction. Proc. Geol. Assoc. 124, 3–82.

Stone, P., 1995. Geology of the Rhinns of Galloway, Memoir of the British Geological Survey. HMSO, London.

Styles, M.T., Gunn, A.G., Rollin, K.E., 2004. A preliminary study of PGE in the Late Caledonian Loch Borralan and Loch Ailsh alkaline pyroxenite-syenite complexes, northwest Scotland. Mineral. Deposita 39, 240–255.

Tanner, P.W.G., 2012. The giant quartz-breccia veins of the Tyndrum-Dalmally area, Grampian Highlands, Scotland: their geometry, origin and relationship to the Cononish gold-silver deposit. Earth and Environmental Science Transactions of the Royal Society of Edinburgh 103, 51–76.

Tanner, P.W.G., Sutherland, S., 2007. The Highland Border Complex, Scotland: a paradox resolved. Journal of the Geological Society of Edinburgh, London 164, 111–116.

Tanner, P.W.G., Thomas, P.R., 2009. Major nappe-like D2 folds in the Dalradian rocks of the Beinn Udlaidh area. Central Highlands, Scotland. Earth and Environmental Science Transactions of the Royal Society of Edinburgh 100, 371–389.

Tarney, J., Jones, C.E., 1994. Trace element geochemistry of orogenic igneous rocks and crustal growth models. J. Geol. Soc. Lond. 151, 855–868.

Tomkins, A.G., 2010. Wetting facilitates late-stage segregation of precious metal-enriched sulfosalt melt in magmatic sulfide systems. Geology 38, 951–954.

Treagus, J.E., Pattrick, R.A.D., Curtis, S.F., 1999. Movement and mineralization in the Tyndrum Fault Zone, Scotland and its regional significance. J. Geol. Soc. Lond. 156, 591–604.

Wagner, T., Boyce, A.J., Fallick, A.E., 2002. Laser combustion analysis of δ34S of sulfosalt minerals: determination of the fractionation systematics and some crystal-chemical considerations. Geochim. Cosmochim. Acta 66, 2855–2863.

Wright, A.E., 1988. The Appin Group. In: Winchester, J.A. (Ed.), Later Proterozoic Stratigraphy of the Northern Atlantic Regions. Blackie, Glasgow.

Yamamoto, M., 1976. Relationship between Se/S and sulfur isotope ratios of hydrothermal sulfide minerals. Mineral. Deposita 11, 197–209.

Ye, H.M., Li, X.H., Li, Z.X., Zhang, C.L., 2008. Age and origin of high Ba-Sr appinite granites at the northwestern margin of the Tibet plateau: implications for early Paleozoic tectonic evolution of the Western Kunlun orogenic belt. Gondwana Res. 13, 126–138.

Zanetti, A., Mazzuccheli, M., Rivalenti, G., Vannucci, R., 1999. The Finero phlogopite-peridotite massif: an example of subduction-related metasomatism. Contrib. Mineral. Petrol. 134, 107–122.